

Phase transitions and gravitational waves in a model of \mathbb{Z}_3 scalar dark matter

Nico Benincasa ^a, Andrzej Hryczuk ^b, Kristjan Kannike ^a and Maxim Laletin ^c

^a*National Institute of Chemical Physics and Biophysics,
Rävala 10, Tallinn, Estonia*

^b*National Centre for Nuclear Research,
Pasteura 7, 02-093 Warsaw, Poland*

^c*Institute of Theoretical Physics, Faculty of Physics, University of Warsaw,
Pasteura 5, 02-093 Warsaw, Poland*

E-mail: nico.benincasa@kbfi.ee, andrzej.hryczuk@ncbj.gov.pl,
Kristjan.Kannike@cern.ch, maxim.laletin@fuw.edu.pl

ABSTRACT: Theories with more than one scalar field often exhibit phase transitions producing potentially detectable gravitational wave (GW) signal. In this work we study the semi-annihilating \mathbb{Z}_3 dark matter model, whose dark sector comprises an inert doublet and a complex singlet, and assess its prospects in future GW detectors. Without imposing limits from requirement of providing a viable dark matter candidate, i.e. taking into account only other experimental and theoretical constraints, we find that the first order phase transition in this model can be strong enough to lead to a detectable signal. However, direct detection and the dark matter thermal relic density constraint calculated with the state-of-the-art method including the impact of early kinetic decoupling, very strongly limit the parameter space of the model explaining all of dark matter *and* providing observable GW peak amplitude. Extending the analysis to underabundant dark matter thus reveals region with detectable GWs from a single-step or multi-step phase transition.

KEYWORDS: Models for Dark Matter, Particle Nature of Dark Matter, Phase Transitions in the Early Universe, Multi-Higgs Models

ARXIV EPRINT: [2312.04627](https://arxiv.org/abs/2312.04627)

Contents

1	Introduction	1
2	\mathbb{Z}_3 dark matter model	3
2.1	Scalar potential and parametrisation	3
2.2	Potential for phase transitions	4
2.2.1	Tree-level potential for phase transitions	4
2.2.2	Quantum corrections to the potential	4
2.2.3	Thermal corrections to the potential	5
2.2.4	Full thermally-corrected effective potential	6
3	Constraints	6
3.1	Perturbativity	6
3.2	Unitarity	6
3.3	Bounded-from-below constraints and globality of the electroweak vacuum	7
3.4	Collider constraints	9
3.5	Electroweak precision parameters	9
4	Relic density	10
5	Phase transition and gravitational waves	15
6	Numerical scan	18
7	Signals	19
7.1	Direct detection	19
7.2	Gravitational waves	19
8	Conclusions	23
A	Field-dependent scalar mass matrices	24
B	Counter-terms	25
C	Sound-wave contribution $h^2\Omega_{\text{sw}}(f)$	25

1 Introduction

Although dark matter (DM) constitutes 27% of the energy density of the Universe [1], its nature is still unknown. The discovery of the Higgs boson, over a decade ago, showed that scalars do exist in nature [2, 3]. In particular, there are two well-motivated candidates of scalar dark matter: the inert doublet [4–7] and the scalar singlet [8–10], usually stabilised by a \mathbb{Z}_2 parity. Both these DM candidates suffer, however, in the face of the most recent

results from the direct detection experiments XENON1T [11], PandaX-4T [12] and LZ [13] that have thus far not seen any evidence of a dark-matter signal.

A possible solution lies in considering a larger scalar dark sector comprising both the inert doublet and a complex singlet with a stabilising symmetry more complex than the \mathbb{Z}_2 parity. In this case, dominant processes that determine the DM relic density can belong to semi-annihilation [14–17] instead of the usual annihilation. Since semi-annihilation and direct-detection processes are driven by different couplings, the correct DM relic density may be obtained while the spin-independent direct-detection cross section lies below the current limits of direct-detection experiments.

In fact, semi-annihilation is possible already for the next-to-simplest stabilising symmetry, the \mathbb{Z}_3 group. In the \mathbb{Z}_3 complex singlet-inert doublet model, the impact of semi-annihilations on DM relic density was first considered in [18] and a comprehensive study of the model was performed in [19].¹ On the other hand, the \mathbb{Z}_3 singlet model [33, 34]² and the inert doublet model [4–7] can be considered as limiting cases of the full model. The \mathbb{Z}_3 singlet model was reconsidered with improved bounds and impact of early kinetic decoupling in [41]. Indirect detection signals have been considered in [42–44] and cosmic phase transitions were considered in [45]. A fit of the \mathbb{Z}_3 singlet model was made in [46]. The \mathbb{Z}_3 singlet-doublet model also shares many constraints with the inert doublet model (IDM) [47–50]. Recent studies of DM phenomenology in the IDM are given by [51–53]. The phase structure of the IDM was studied in [54]. First-order phase transitions in the IDM were studied in [55–59] and the GW phenomenology of the inert doublet model was elucidated in [60]. IDM, augmented by higher-order operators, can also give rise to baryogenesis [61]. Notably, \mathbb{Z}_3 symmetry and semi-annihilation have also been considered for a singlet-extended type II seesaw model [62].

In the part of the parameter space where semi-annihilation dominates, one has to take extra care in calculating the DM relic density. In the standard calculation of the thermal relic abundance [63] it is assumed that, at the freeze-out, DM is still in equilibrium with the heat bath. Indeed, usually the elastic scattering processes with the thermal bath particles are much more efficient than the processes of annihilation and production. If the latter are enhanced, however, or if the scattering processes are not related to the number changing ones — which is the case for semi-annihilation — this assumption may not be satisfied. It has been shown that kinetic decoupling can begin as early as the chemical one and that the change in the DM phase space distribution may modify the relic abundance by more than an order of magnitude [64–66].

Although direct detection of DM remains elusive, other observational channels are becoming available. The discovery of gravitational waves (GW) by the LIGO experiment [67, 68] has begun a new era of GW astronomy. Of particular interest to particle physicists is the possibility to probe the vacuum structure of the scalar potential via cosmic phase

¹The \mathbb{Z}_2 model with the same field content was studied in [20–23]. More complicated symmetries may further restrict possible interactions: see e.g. [24] and [25]. With a \mathbb{Z}_4 symmetry one can have two-component dark matter for the same field content [18, 19, 26, 27] (see also e.g. [28–31] for generalisations). With higher symmetries, such as \mathbb{Z}_7 , and more fields, one can have even three-component DM [32].

²It is possible that the \mathbb{Z}_3 symmetry is a remnant of breaking of a $U(1)$ group, see e.g. [35–38]. On the other hand, if the \mathbb{Z}_3 symmetry itself is broken, but the CP symmetry is conserved, the pseudoscalar part of the complex singlet is still stable and can be a DM candidate [39, 40].

transitions. In the SM, the phase transition is a smooth cross-over [69, 70] which does not produce a GW signal. A larger scalar sector in an extension of the SM, however, can give rise to first-order phase transitions [71–73] which can produce a stochastic GW background that could be detected by future GW detectors such as LISA [74, 75], BBO [76, 77], Taiji [78, 79], TianQin [80] or DECIGO [81, 82] (see e.g. ref. [83] for a pedagogical review).

The aims of this paper are therefore twofold: first of all to study gravitational-wave signals originating during phase transitions predicted by the inert doublet-singlet model with a \mathbb{Z}_3 symmetry and, second, to update the phenomenological analysis of this model by including constraints from vacuum stability, unitarity and perturbativity, and electroweak precision parameters and calculating the thermal relic density taking into account the effects of early kinetic decoupling.

The paper is organised as follows. We describe the tree-level scalar potential of the model together with the loop and thermal corrections in section 2. Various theoretical and experimental constraints are given in section 3. Relic density calculation with early kinetic decoupling is discussed in section 4. Calculations of phase transitions and the gravitational-wave signal are elucidated in section 5. Our Monte Carlo scan is described in section 6 and the signals in section 7. We conclude in section 8. Appendices list field-dependent scalar masses (A), effective potential counter-terms (B) and formulae for the sound-wave contribution to the gravitational-wave signal (C).

2 \mathbb{Z}_3 dark matter model

2.1 Scalar potential and parametrisation

Our scalar fields comprise, besides the Standard-Model Higgs boson H_1 , an inert doublet H_2 and a complex singlet S . Dark matter is made stable thanks to a \mathbb{Z}_3 discrete symmetry under which the Higgs boson, together with all other SM fields, transforms trivially: $H_1 \rightarrow H_1$, $S \rightarrow \omega S$, $H_2 \rightarrow \omega H_2$ with $\omega^3 = 1$ (considering $S \rightarrow \omega^2 S$, $H_2 \rightarrow \omega^2 H_2$ is equivalent). The most general scalar potential invariant under the \mathbb{Z}_3 is given by [18, 19]

$$\begin{aligned}
 V = & \mu_1^2 |H_1|^2 + \lambda_1 |H_1|^4 + \mu_2^2 |H_2|^2 + \lambda_2 |H_2|^4 + \mu_S^2 |S|^2 + \lambda_S |S|^4 \\
 & + \lambda_{S1} |S|^2 |H_1|^2 + \lambda_{S2} |S|^2 |H_2|^2 + \lambda_3 |H_1|^2 |H_2|^2 + \lambda_4 (H_1^\dagger H_2)(H_2^\dagger H_1) \\
 & + \frac{\mu_S''}{2} (S^3 + S^{\dagger 3}) + \frac{\lambda_{S12}}{2} (S^2 H_1^\dagger H_2 + S^{\dagger 2} H_2^\dagger H_1) + \frac{\mu_{SH}}{2} (S H_2^\dagger H_1 + S^\dagger H_1^\dagger H_2),
 \end{aligned}
 \tag{2.1}$$

where we take all the parameters real. We can parametrise the fields in the EW vacuum in the Landau gauge as

$$H_1 = \begin{pmatrix} G^+ \\ \frac{v+h+iG^0}{\sqrt{2}} \end{pmatrix}, \quad H_2 = \begin{pmatrix} H^+ \\ \frac{H+iA}{\sqrt{2}} \end{pmatrix}, \quad S = \frac{s+i\chi}{\sqrt{2}},
 \tag{2.2}$$

where $v = 246.22$ GeV is the vacuum expectation value (VEV) of the SM Higgs field H_1 at zero temperature.

Notice that the absence of the term $\lambda_5 [(H_1^\dagger H_2)^2 + (H_2^\dagger H_1)^2]$ — forbidden by the \mathbb{Z}_3 symmetry — means that there is no mass splitting between the scalar component H and pseudoscalar component A of the neutral part of H_2 . The μ_{SH} term in the above potential

induces a mixing by an angle θ between S and the neutral part of H_2 . In terms of the complex mass eigenstates x_1 and x_2 , it yields

$$\frac{H + iA}{\sqrt{2}} = x_1 \sin \theta + x_2 \cos \theta \quad \text{and} \quad \frac{s + i\chi}{\sqrt{2}} = x_1 \cos \theta - x_2 \sin \theta. \quad (2.3)$$

Because x_2 is doublet-like and has gauge interactions with the Z boson, it cannot be a DM candidate due to its large direct detection cross section. Therefore, we always consider $M_{x_1} < M_{x_2}$ and choose the singlet-like x_1 as our DM candidate.

We then express the parameters in eq. (2.1) in terms of the physical masses M_h , M_{x_1} , M_{x_2} , M_{H^\pm} , the dark sector mixing angle θ and the Higgs VEV v :

$$\begin{aligned} \mu_1^2 &= -\frac{M_h^2}{2}, \quad \mu_2^2 = M_{H^\pm}^2 - \frac{\lambda_3 v^2}{2}, \quad \mu_S^2 = M_{x_1}^2 \cos^2 \theta + M_{x_2}^2 \sin^2 \theta - \frac{\lambda_{S1} v^2}{2}, \\ \mu_{SH} &= \frac{\sqrt{2}}{v} (M_{x_1}^2 - M_{x_2}^2) \sin 2\theta, \quad \lambda_1 = \frac{M_h^2}{2v^2}, \quad \lambda_4 = \frac{2}{v^2} (M_{x_1}^2 \sin^2 \theta + M_{x_2}^2 \cos^2 \theta - M_{H^\pm}^2). \end{aligned} \quad (2.4)$$

2.2 Potential for phase transitions

2.2.1 Tree-level potential for phase transitions

When dealing with phase transitions and gravitational-wave signals in subsection 7.2, we consider the path to tunnel from the origin to the EW minimum to lie in the three-dimensional field space of h, H and s . Therefore in the potential (2.1) we set all other scalar fields to zero. The resulting tree-level potential is thus

$$\begin{aligned} V_{\text{cl}}(h, H, s) &= \frac{\mu_1^2}{2} h^2 + \frac{\lambda_1}{4} h^4 + \frac{\mu_2^2}{2} H^2 + \frac{\lambda_2}{4} H^4 + \frac{\mu_S^2}{2} s^2 + \frac{\lambda_S}{4} s^4 + \frac{\lambda_3 + \lambda_4}{4} h^2 H^2 \\ &+ \frac{\lambda_{S1}}{4} h^2 s^2 + \frac{\lambda_{S2}}{4} H^2 s^2 + \frac{\lambda_{S12}}{4} h H s^2 + \frac{\mu_S''}{2\sqrt{2}} s^3 + \frac{\mu_{SH}}{2\sqrt{2}} h H s. \end{aligned} \quad (2.5)$$

2.2.2 Quantum corrections to the potential

The Coleman-Weinberg potential contains the quantum corrections to the tree-level potential (2.5) given by the sum of the one-particle-irreducible diagrams with external lines from amongst the classical background fields h, H and s . The one-loop Coleman-Weinberg potential is expressed in the Landau gauge as [84]

$$\Delta V(h, H, s) = \frac{1}{64\pi^2} \sum_i n_i m_i^4 \left(\ln \frac{m_i^2}{\mu^2} - C_i \right), \quad (2.6)$$

where the sum ranges over the fields $i = W_T^\pm, W_L^\pm, Z_T, Z_L, \gamma_L, t, h, H, s, G_0, A, \chi, G^\pm, H^\pm$. We neglect the lighter fermions because their Yukawa couplings are very small as compared to the top Yukawa. We choose the renormalisation scale to be $\mu = v$, and C_i are constants peculiar to the renormalisation scheme. The subscripts T and L , respectively, denote the transverse and longitudinal components of the gauge bosons. The bosonic and fermionic degrees of freedom³ are given by $n_{W_T^\pm} = 4, n_{W_L^\pm} = 2, n_{Z_T} = 2, n_{Z_L} = 1, n_{\gamma_L} = 1, n_t =$

³Strictly speaking, talking about degrees of freedom n_W, n_Z for the massive gauge bosons is an abuse of notation; the fortuitous correspondence between their value and the number of polarisation states is not true in every gauge [85].

$-12, n_h = n_H = n_s = n_{G_0} = n_A = n_\chi = 1$ and $n_{H^\pm} = n_{G^\pm} = 2$. The constants $C_i = 3/2$ for scalars, fermions and longitudinal vector bosons, as well as $C_i = 1/2$ for transverse vector bosons in the $\overline{\text{MS}}$ subtraction scheme. The field-dependent scalar masses $m_i^2 \equiv m_i^2(h, H, s)$ correspond to the eigenvalues of the field-dependent mass matrices of the scalar fields M_S^2 , of the pseudoscalar fields M_P^2 and of the charged fields M_C^2 , which are given in the appendix A. The field-dependent top quark and gauge boson masses are given by

$$m_t^2 = \frac{y_t^2}{2} h^2, \quad m_{W_T^\pm}^2 = m_{W_L^\pm}^2 = \frac{g_2^2}{4} (h^2 + H^2), \quad m_{Z_T}^2 = m_{Z_L}^2 = \frac{g_1^2 + g_2^2}{4} (h^2 + H^2), \quad m_{\gamma_L}^2 = 0, \quad (2.7)$$

where y_t , g_1 and g_2 are the top Yukawa coupling, the $U(1)_Y$ and $SU(2)_L$ gauge couplings, respectively.

In order to fix the masses, VEV and the dark sector mixing angle at their tree-level values, we cancel contributions from the one-loop ΔV in the EW vacuum with opposite-sign contributions from the counterterm potential given by

$$\begin{aligned} \delta V(h, H, s) = & \delta\mu_1^2 h^2 + \delta\mu_2^2 H^2 + \delta\mu_S^2 s^2 + \delta\lambda_1 h^4 + (\delta\lambda_3 + \delta\lambda_4) h^2 H^2 \\ & + \delta\lambda_{S1} h^2 s^2 + \delta\lambda_{S12} h H s^2 + \delta\mu_S'' s^3 + \delta\mu_{SH} h H s, \end{aligned} \quad (2.8)$$

whose coefficients are given in the appendix B. This cancellation is guaranteed by the following set of renormalisation conditions:

$$\begin{aligned} \partial_h (\Delta V + \delta V) \Big|_{\text{VEV}} = 0, \quad \partial_{h^2}^2 (\Delta V + \delta V) \Big|_{\text{VEV}} = 0, \quad \partial_{H^2}^2 (\Delta V + \delta V) \Big|_{\text{VEV}} = 0, \\ \partial_{s^2}^2 (\Delta V + \delta V) \Big|_{\text{VEV}} = 0, \quad \partial_H \partial_s (\Delta V + \delta V) \Big|_{\text{VEV}} = 0, \quad \partial_h \partial_{H^2}^2 (\Delta V + \delta V) \Big|_{\text{VEV}} = 0, \\ \partial_h \partial_{s^2}^2 (\Delta V + \delta V) \Big|_{\text{VEV}} = 0, \quad \partial_H \partial_{s^2}^2 (\Delta V + \delta V) \Big|_{\text{VEV}} = 0, \quad \partial_{s^3}^3 (\Delta V + \delta V) \Big|_{\text{VEV}} = 0, \end{aligned} \quad (2.9)$$

where VEV means at the EW minimum $(h, H, s) = (v, 0, 0)$. In eq. (2.9), we take care of the problematic IR divergence occurring in $\ln m_G^2$ (due to the vanishing Goldstone mass in the EW vacuum) by replacing m_G with M_h [86] as an infrared regulator.

2.2.3 Thermal corrections to the potential

The one-loop finite-temperature contribution to the effective potential is given by [87]

$$V_T(h, H, s, T) = \frac{T^4}{2\pi} \sum_i n_i J_{\text{B/F}} \left(\frac{m_i^2}{T^2} \right), \quad (2.10)$$

where the thermal bosonic/fermionic functions $J_{\text{B/F}}$ are defined as [87]

$$J_{\text{B/F}}(y^2) = \int_0^\infty dx x^2 \ln \left(1 \mp e^{-\sqrt{x^2 + y^2}} \right). \quad (2.11)$$

It is customary to deal with IR divergences arising from the zero bosonic Matsubara mode in the high-temperature limit by considering the so-called daisy resummation [88]. This procedure amounts to adding the leading-order thermal correction or Debye mass $\Pi_i T^2$ to the mass m_i^2 in ΔV and V_T [89]. For the scalar sector it means

$$\mu_i^2 \rightarrow \mu_i^2 + c_i T^2 \quad \text{with} \quad i = 1, 2, S, \quad (2.12)$$

where

$$c_1 = \frac{1}{16}(g_1^2 + 3g_2^2 + 4y_t^2) + \frac{1}{12}(6\lambda_1 + 2\lambda_3 + \lambda_4 + \lambda_{S1}), \quad (2.13)$$

$$c_2 = \frac{1}{16}(g_1^2 + 3g_2^2) + \frac{1}{12}(6\lambda_2 + 2\lambda_3 + \lambda_4 + \lambda_{S2}), \quad (2.14)$$

$$c_S = \frac{1}{6}(2\lambda_S + \lambda_{S1} + \lambda_{S2}) \quad (2.15)$$

with the SM contribution taken from [90]. There is no need to consider the thermal mass of the top quark and fermions in general, because daisy diagrams do not diverge in the IR, since there is no zero Matsubara frequency for fermions [91–93]. As for gauge bosons, only their longitudinal modes acquire a significant thermal correction to their mass, thereby the Debye mass of transverse modes (protected by gauge symmetry) is neglected [91, 94, 95].

Notice that thermal contributions to the longitudinal part of Z and γ should be added to their mass matrix in the gauge basis before it is diagonalised. The Debye mass of W_L is $\Pi_{W_L} T^2 = 2g_2^2 T^2$, while for Z_L and γ_L , one should add

$$\text{diag}(c_Z T^2, c_\gamma T^2), \quad \text{with} \quad c_Z = 2g_2^2, \quad c_\gamma = 2g_1^2 \quad (2.16)$$

to their mass matrix and then diagonalise it [91, 96].

2.2.4 Full thermally-corrected effective potential

The full thermally-corrected effective potential needed to compute phase-transition parameters is thus made of the classical potential (2.5), to which one adds quantum corrections summarised in (2.6) and (2.8), as well as thermal corrections (2.10):

$$V_{\text{eff}}(h, H, s, T) = V_{\text{cl}}(h, H, s) + V_{\text{CW}}(h, H, s, T) + \delta V(h, H, s) + V_{\text{T}}(h, H, s, T). \quad (2.17)$$

3 Constraints

3.1 Perturbativity

We require the Feynman rule vertex factors of quartic interactions to be less than 4π in absolute value to ensure that the one-loop contributions be smaller than tree-level ones [97]. This yields the conditions

$$\begin{aligned} |\lambda_1| < \frac{2\pi}{3}, \quad |\lambda_2| < \pi, \quad |\lambda_3| < 4\pi, \quad |\lambda_4| < 4\sqrt{2}\pi, \quad |\lambda_3 + \lambda_4| < 4\pi, \\ |\lambda_S| < \pi, \quad |\lambda_{S1}| < 4\pi, \quad |\lambda_{S2}| < 4\pi, \quad |\lambda_{S12}| < 4\pi. \end{aligned} \quad (3.1)$$

3.2 Unitarity

The cross section of $2 \rightarrow 2$ scattering processes $s_1 s_2 \rightarrow s_3 s_4$ of scalars s_i can be expanded in the partial wave decomposition as

$$\sigma = \frac{16\pi}{s} \sum_{l=1}^{\infty} (2l+1) |a_l(s)|^2, \quad (3.2)$$

where s is the Mandelstam variable and a_l are the partial wave coefficients with the angular momenta l . The optical theorem imposes on a_l the unitarity bound

$$|\Re(a_l)| < \frac{1}{2}. \quad (3.3)$$

In the high energy limit, the s -wave amplitude $a_0(s)$ is dominated by contact terms because the s -, t - and u -channel processes are suppressed by the scattering energy. Therefore, in the high energy limit, $a_0(s)$ is completely determined by the quartic couplings of the scalar potential. The constraint (3.3) places an upper bound on the eigenvalues of the $2 \rightarrow 2$ scalar scattering matrix. The unitarity bounds of the 2HDM were first studied in [98, 99]. For the \mathbb{Z}_3 scalar quartic couplings, the unitarity bounds are given by⁴

$$|\lambda_1| \leq 4\pi, \quad (3.4)$$

$$|\lambda_2| \leq 4\pi, \quad (3.5)$$

$$|\lambda_3| \leq 8\pi, \quad (3.6)$$

$$|\lambda_3 - \lambda_4| \leq 8\pi, \quad (3.7)$$

$$|\lambda_3 + \lambda_4| \leq 8\pi, \quad (3.8)$$

$$\left| \lambda_1 + \lambda_2 \pm \sqrt{(\lambda_1 - \lambda_2)^2 + \lambda_4^2} \right| \leq 8\pi, \quad (3.9)$$

$$\left| \lambda_3 + 2\lambda_4 + 2\lambda_S \pm \sqrt{(\lambda_3 + 2\lambda_4 - 2\lambda_S)^2 + 4\lambda_{S12}^2} \right| \leq 16\pi, \quad (3.10)$$

$$|\lambda_{S1}| \leq 8\pi, \quad (3.11)$$

$$|\lambda_{S2}| \leq 8\pi, \quad (3.12)$$

$$\left| \lambda_{S1} + \lambda_{S2} \pm \sqrt{(\lambda_{S1} - \lambda_{S2})^2 + 4\lambda_{S12}^2} \right| \leq 16\pi \quad (3.13)$$

and $|\Lambda_i| \leq 1/2$, where the three remaining eigenvalues Λ_i with $i = 1, 2, 3$ of the scattering matrix are given by the solution of the cubic equation

$$\begin{aligned} x^3 + \frac{1}{8\pi}x^2(3\lambda_1 + 3\lambda_2 + 2\lambda_S) + \frac{1}{256\pi^2}x(36\lambda_1\lambda_2 - 4\lambda_3^2 - 4\lambda_3\lambda_4 - \lambda_4^2 + 24\lambda_1\lambda_S + 24\lambda_2\lambda_S \\ - 2\lambda_{S1}^2 - 2\lambda_{S2}^2) + \frac{1}{1024\pi^3}(36\lambda_1\lambda_2\lambda_S - 4\lambda_3^2\lambda_S - 4\lambda_3\lambda_4\lambda_S - \lambda_4^2\lambda_S - 3\lambda_2\lambda_{S1}^2 + 2\lambda_3\lambda_{S1}\lambda_{S2} \\ + \lambda_4\lambda_{S1}\lambda_{S2} - 3\lambda_1\lambda_{S2}^2) = 0. \end{aligned} \quad (3.14)$$

3.3 Bounded-from-below constraints and globality of the electroweak vacuum

In order to be physical, the potential has to be bounded from below in the limit of large field values. In this limit, the dimensionful quadratic and cubic terms can be neglected — it suffices to consider only the quartic part of the potential (2.1). The analytical necessary and sufficient bounded-from-below constraints were derived in ref. [100]. We only sketch the derivation and refer the reader to that paper for details and ancillary *Mathematica* code.

⁴We correct the result in [19], where an overall factor of 2 is missing from the scattering matrix and the coupling λ_S should be replaced with $2\lambda_S$.

The potential (2.1), using the parameterisation

$$|H_1|^2 = h_1^2, \quad |H_2|^2 = h_2^2, \quad H_1^\dagger H_2 = h_1 h_2 \rho e^{i\phi}, \quad S = s e^{i\phi_S}, \quad (3.15)$$

where $0 \leq \rho \leq 1$ as implied by the Cauchy inequality $0 \leq |H_1^\dagger H_2| \leq |H_1||H_2|$, and $0 \leq \phi, \phi_S < 2\pi$, takes the form

$$V = \lambda_1 h_1^4 + \lambda_2 h_2^4 + \lambda_3 h_1^2 h_2^2 + \lambda_4 \rho^2 h_1^2 h_2^2 + \lambda_S s^4 + \lambda_{S1} s^2 h_1^2 + \lambda_{S2} s^2 h_2^2 - |\lambda_{S12}| \rho s^2 h_1 h_2, \quad (3.16)$$

where we have minimised $\cos(\phi + 2\phi_S + \phi_{\lambda_{S12}}) = -1$ so $\lambda_{S12} = -|\lambda_{S12}|$ without loss of generality. We have to minimise the potential with respect to ρ , also taking into account separately the ends $\rho = 0$ and $\rho = 1$ of the interval. The conditions for $s = 0$ or $\rho = 0$ are given by

$$\begin{aligned} \lambda_1 &> 0, & \lambda_2 &> 0, & \lambda_S &> 0, \\ \bar{\lambda}_3 &\equiv \lambda_3 + 2\sqrt{\lambda_1 \lambda_2} > 0, & \bar{\lambda}_{34} &\equiv \lambda_3 + \lambda_4 + 2\sqrt{\lambda_1 \lambda_2} > 0, \\ \bar{\lambda}_{S1} &\equiv \lambda_{S1} + 2\sqrt{\lambda_S \lambda_1} > 0, & \bar{\lambda}_{S2} &\equiv \lambda_{S2} + 2\sqrt{\lambda_S \lambda_2} > 0 \\ & & \sqrt{\lambda_S \lambda_3} + \sqrt{\lambda_1 \lambda_{S2}} + \sqrt{\lambda_2 \lambda_{S1}} + \sqrt{\lambda_S \lambda_1 \lambda_2} + \sqrt{\bar{\lambda}_{S1} \bar{\lambda}_{S2} \bar{\lambda}_3} &> 0. \end{aligned} \quad (3.17)$$

Another necessary but not sufficient (since it is calculated with $\rho = 1$, but ignoring the λ_{S12} term) condition can be given by

$$\sqrt{\lambda_S}(\lambda_3 + \lambda_4) + \sqrt{\lambda_1} \lambda_{S2} + \sqrt{\lambda_2} \lambda_{S1} + \sqrt{\lambda_S \lambda_1 \lambda_2} + \sqrt{\bar{\lambda}_{S1} \bar{\lambda}_{S2} \bar{\lambda}_{34}} > 0. \quad (3.18)$$

We minimise the potential with respect to h_1, h_2, s and ρ with the fields lying on a sphere, enforced by a Lagrange multiplier λ . The minimisation equations with respect to the fields and λ are

$$\begin{aligned} 4\lambda_1 h_1^3 + 2(\lambda_3 + \lambda_4 \rho^2) h_1 h_2^2 + 2\lambda_{S1} h_1 s^2 - |\lambda_{S12}| \rho h_2 s^2 &= \lambda h_1, \\ 4\lambda_2 h_2^3 + 2(\lambda_3 + \lambda_4 \rho^2) h_1^2 h_2 + 2\lambda_{S2} h_2 s^2 - |\lambda_{S12}| \rho h_1 s^2 &= \lambda h_2, \\ s(4\lambda_S s^2 + 2\lambda_{S1} h_1^2 + 2\lambda_{S2} h_2^2 - 2|\lambda_{S12}| \rho h_1 h_2) &= \lambda s, \\ h_1^2 + h_2^2 + s^2 &= 1. \end{aligned} \quad (3.19)$$

and the minimisation equation with respect to ρ is

$$h_1 h_2 (2\rho \lambda_4 h_1 h_2 - |\lambda_{S12}| s^2) = 0, \quad (3.20)$$

The equations (3.19) and (3.20), solved together, have an analytical solution. The bounded-from-below conditions for $0 < \rho < 1$ are then given by

$$0 < h_1^2 < 1 \wedge 0 < h_2^2 < 1 \wedge 0 < s^2 < 1 \wedge 0 < \rho^2 < 1 \implies V_{\min} > 0, \quad (3.21)$$

where V_{\min} , the value of minimum at the solution, is proportional to the Lagrange multiplier λ . Note that $p \implies q$ is equivalent to $\neg p \vee q$. In addition, the equations (3.19) need also to be solved with $\rho = 1$, in which case the conditions are given by⁵

$$0 < h_1 < 1 \wedge 0 < h_2 < 1 \wedge 0 < s < 1 \implies V_{\min} > 0. \quad (3.22)$$

⁵Another form of these conditions is given in ref. [100].

The necessary and sufficient bounded-from-below conditions are then given by eqs. (3.17), (3.21) and (3.22). Eq. (3.18) can be used for faster elimination of invalid points.

Once the bounded-from-below conditions are satisfied, the potential is guaranteed to have a finite global minimum solution. Although it is possible that our EW vacuum, not coinciding with the global one, is metastable, the gain in the parameter space is expected to be marginal (at least in the singlet-like case [41]). For that reason, we simply demand that the EW vacuum be the global one.

3.4 Collider constraints

The LEP collider measured to high precision the decay widths of the Z and W bosons, which are compatible with the SM. Neglecting the small mixing between the singlet and doublet, we require that the particle masses satisfy [101]

$$M_{x_2} + M_{H^\pm} > M_W, \quad 2M_{x_2} > M_Z, \quad 2M_{H^\pm} > M_Z. \quad (3.23)$$

LEP searches for new neutral final states further exclude a range of masses [102], thereby forcing

$$m_H > 80 \text{ GeV}, \quad m_A > 100 \text{ GeV} \quad \text{or} \quad m_A - m_H < 8 \text{ GeV}, \quad (3.24)$$

in addition to

$$m_{H^\pm} > 70 \text{ GeV} \quad (3.25)$$

due to searches for charged scalar pair production [103]. But since there is no splitting between m_H and m_A , the constraint (3.24) is always satisfied.

Similarly, if $M_{x_1} < M_h/2$ or $M_{x_2} < M_h/2$, the Higgs boson can decay into dark sector. This is constrained by measurements of the Higgs boson invisible branching ratio $\text{BR}_{\text{inv}} = \Gamma_{h \rightarrow x_1 x_1} / (\Gamma_{h \rightarrow \text{SM}} + \Gamma_{h \rightarrow x_1 x_1})$. Latest measurements by the CMS experiment at the LHC find that $\text{BR}_{h \rightarrow \text{inv}} < 0.15$ [104], while the ATLAS experiment measures $\text{BR}_{h \rightarrow \text{inv}} < 0.11$ [105], of which we will require the stricter ATLAS constraint.

We also use the micrOMEGAs package to compute the $h \rightarrow \gamma\gamma$ decay rate (usually similar to the IDM one [47, 48]) and require it to be within the value measured at the CMS [106]: $\mu_{h \rightarrow \gamma\gamma} = 1.12 \pm 0.09$.

3.5 Electroweak precision parameters

The measurements of electroweak precision data at the LEP put strong constraints on physics beyond the SM. The latest electroweak fit by the Gfitter group [107] gives for the oblique parameters S and T (with $U = 0$) the central values

$$S = 0.04 \pm 0.08, \quad T = 0.08 \pm 0.14, \quad (3.26)$$

with a correlation coefficient of +0.92.

To calculate electroweak precision parameters S and T , we use the results for general models with doublets and singlets [108, 109]. The usual loop functions are defined as

$$F(I, J) = \frac{I + J}{2} - \frac{IJ}{I - J} \ln \frac{I}{J}, \quad (3.27)$$

with $F(I, I) = 0$ in the limit of $J \rightarrow I$, and

$$G(I, J, Q) = -\frac{16}{3} + \frac{5(I+J)}{Q} - \frac{2(I-J)^2}{Q^2} + \frac{3}{Q} \left[\frac{I^2+J^2}{I-J} - \frac{I^2-J^2}{Q} + \frac{(I-J)^3}{3Q^2} \right] \ln \frac{I}{J} + \frac{r}{Q^3} f(t, r), \quad (3.28)$$

where

$$t \equiv I + J - Q \quad \text{and} \quad r \equiv Q^2 - 2Q(I + J) + (I - J)^2, \quad (3.29)$$

$$f(t, r) \equiv \begin{cases} \sqrt{r} \ln \left| \frac{t-\sqrt{r}}{t+\sqrt{r}} \right| & \Leftarrow r > 0, \\ 0 & \Leftarrow r = 0, \\ 2\sqrt{-r} \arctan \frac{\sqrt{-r}}{t} & \Leftarrow r < 0. \end{cases} \quad (3.30)$$

The beyond-the-SM contributions to the S and T parameters are given by

$$\begin{aligned} \Delta S &= \frac{1}{24\pi} \left[(2s_W^2 - 1)^2 G(M_{H^\pm}^2, M_{H^\pm}^2, M_Z^2) + \cos^4 \theta G(M_{x_2}^2, M_{x_2}^2, M_Z^2) \right. \\ &\quad + 2 \sin^2 \theta \cos^2 \theta G(M_{x_1}^2, M_{x_2}^2, M_Z^2) + \sin^4 \theta G(M_{x_1}^2, M_{x_1}^2, M_Z^2) \\ &\quad \left. + 2 \sin^2 \theta \ln M_{x_1}^2 + 2 \cos^2 \theta \ln M_{x_2}^2 - 2 \ln M_{H^\pm}^2 \right] \\ &\approx \frac{1}{24\pi} \left[(2s_W^2 - 1)^2 G(M_{H^\pm}^2, M_{H^\pm}^2, M_Z^2) + G(M_{x_2}^2, M_{x_2}^2, M_Z^2) \right. \\ &\quad \left. + 2 \ln M_{x_2}^2 - 2 \ln M_{H^\pm}^2 \right], \end{aligned} \quad (3.31)$$

and

$$\begin{aligned} \Delta T &= \frac{1}{16\pi^2 \alpha v^2} \left[\sin^2 \theta F(M_{H^\pm}^2, M_{x_1}^2) + \cos^2 \theta F(M_{H^\pm}^2, M_{x_2}^2) \right. \\ &\quad \left. - \sin^2 \theta \cos^2 \theta F(M_{x_1}^2, M_{x_2}^2) \right] \\ &\approx \frac{1}{16\pi^2 \alpha v^2} F(M_{H^\pm}^2, M_{x_2}^2), \end{aligned} \quad (3.32)$$

where the approximations are given for a small mixing angle. The electroweak precision constraints mean that M_{H^\pm} cannot be too different from M_{x_2} . We require the S and T parameters to fall within the 95% C.L. ellipse.

4 Relic density

The cosmological abundance of DM measured by the Planck satellite $\Omega_c h^2 = 0.120 \pm 0.001$ [1] significantly constrains the allowed parameter space of the model. The model that we study contains a non-trivial dark sector that is comprised of several particles with \mathbb{Z}_3 quantum numbers: x_1 , x_2 and H^\pm . Among them only the singlet-like x_1 can play the role of DM, since the physical states that originate from the inert doublet H_2 are too strongly coupled to the SM fields to satisfy the constraints and requirements for the DM candidate. Nevertheless, the processes that involve other dark sector particles in the early Universe can leave an imprint

on the relic abundance and generally has to be included in the calculation of DM density evolution. In similar models with semi-annihilation [18, 19, 26, 110], the relic density is obtained under the assumption that all the particles were initially in thermal equilibrium with the SM plasma and furthermore that the kinetic equilibrium is maintained throughout the whole DM production stage. In this case the density of DM can be obtained by solving the set of Boltzmann equations for the densities of different particles in the dark sector, e.g. using available numerical solvers like micrOMEGAs [111–113] that can work with multi-component DM models [114]. If the processes of DM scattering on the SM plasma particles are not very efficient, the kinetic decoupling can occur before the freeze-out. In this case semi-annihilation processes can redistribute the energy of DM particles and modify its temperature,⁶ which has an impact on the rates of annihilation processes. Although this assumption is often justified or introduces very small corrections to the relic density, in some regimes the process that defines the dynamics of the freeze out can be strongly velocity-dependent, e.g. due to a resonance or s -wave suppression, so that its rate becomes sensitive to the temperature of DM. The density evolution of \mathbb{Z}_3 scalar singlet DM with semi-annihilation beyond the assumption of kinetic equilibrium was studied in ref. [41]. In this work we use the same method to calculate the relic density, but extend it to the multi-component case of the model that we study and include additional interactions present in this model.

In order to properly take into account the departure from kinetic equilibrium of the DM particles and its effect on the relic abundances, we follow the formalism of [64] and the numerical implementation as presented in the DRAKE code release paper [66], with the addition of semi-annihilation collision term as discussed in [41]. We focus on the cBE method, i.e. coupled Boltzmann equations for the 0th and 2nd moment of the distribution function, describing the evolution of number density and temperature, respectively. In doing so we neglect potential corrections from the departure of the thermal shape of the DM distribution.⁷ Below we briefly review the adopted formalism.

The formulation of the system of Boltzmann equations that we solve originates from the master equation governing the evolution of the phase-space density $f_i = f_i(t, \mathbf{p})$ of particle i in an expanding Friedmann-Lemaître-Robertson-Walker universe:

$$E (\partial_t - H \mathbf{p} \cdot \nabla_{\mathbf{p}}) f_i = C[f_i], \tag{4.1}$$

where H is the Hubble parameter and the collision term $C[f_i]$ contains all possible binary and non-binary interactions between dark sector and/or SM particles. Taking the first two moments of the above equation, i.e. integrating it over $g_i \int d^3p/(2\pi)^3/E$ and $g_i \int d^3p/(2\pi)^3 \mathbf{p}^2/E^2$, respectively, with g_i being the number of spin degrees of freedom, and introducing

⁶Here we consider a simplified picture of DM evolution, which holds on the assumption that the DM distribution has an equilibrium *shape*, leading to coupled Boltzmann equations (cBE) for the moments of the distribution function. In general one has to solve the full Boltzmann equation (fBE) for the DM distribution function as described in ref. [66], however in this work we follow the assumption above.

⁷These are expected to be sub-leading and their proper calculation would require much more complicated calculation involving not only self-interaction processes [115], but also an implementation of the semi-annihilation collision term at the phase-space level, which is considerably more CPU expensive.

new variables $Y \equiv n/s$ and $y \equiv \frac{m_\chi}{3s^{2/3}} \left\langle \frac{\mathbf{p}^2}{E} \right\rangle$ with $x = m_{x_1}/T$, one finds:

$$\frac{Y'_i}{Y_i} = \frac{m_i}{x\tilde{H}} C_0, \tag{4.2}$$

$$\frac{y'_i}{y_i} = \frac{m_i}{x\tilde{H}} C_2 - \frac{Y'_i}{Y_i} + \frac{H}{x\tilde{H}} \frac{g_i}{3n_i T_i} \int \frac{d^3p}{(2\pi)^3} \frac{\mathbf{p}^4}{E^3} f_i(\mathbf{p}), \tag{4.3}$$

where we introduce the moments of the collision term as

$$m_i n_i C_0 \equiv g_i \int \frac{d^3p}{(2\pi)^3 E} C[f_i], \tag{4.4}$$

$$m_i n_i \left\langle \frac{\mathbf{p}^2}{E} \right\rangle C_2 \equiv g_i \int \frac{d^3p}{(2\pi)^3 E} \frac{\mathbf{p}^2}{E} C[f_i]. \tag{4.5}$$

This set of cBE (4.2) and (4.3) is not closed in terms of higher moments unless some assumption is made on the form of the distribution function. A well motivated one is to make an ansatz

$$f_i(E_i, T_i) = \frac{n_i(T_i)}{n_i^{\text{eq}}(T_i)} e^{-E_i/T_i}, \tag{4.6}$$

which enforces the Maxwell-Boltzmann shape, but with an arbitrary temperature T_i . In the scenario studied in this work we have $i \in \{x_1, x_2, H^\pm\}$, but we will make a simplifying assumption that only the DM particle, x_1 , has a population which departs from kinetic equilibrium, while all three dark sector states can depart from chemical equilibrium. This assumption is justified as x_2 and H^\pm are relatively tightly coupled to the thermal bath, leading to their kinetic decoupling happening well after all the freeze-out processes take place, while in the regions of dominant semi-annihilation the x_1 has suppressed elastic scatterings and thus can undergo an early kinetic decoupling.

The general expression for the collision term for i -th particle due to binary collisions reads

$$C = \frac{1}{2g_i} \sum_{j\{kl\}} \frac{1}{(1 + \delta_{kl})} \int d\Pi_j d\Pi_k d\Pi_l (2\pi)^4 \delta^{(4)}(p_i + p_j - p_k - p_l) \left| \bar{M} \right|_{ij \leftrightarrow kl}^2 \times [f_k f_l (1 \pm f_i)(1 \pm f_j) - f_i f_j (1 \pm f_k)(1 \pm f_l)], \tag{4.7}$$

where the sum goes over all possible j and two-particle $\{kl\}$ states, with and without the DM, and $\left| \bar{M} \right|^2$ is the amplitude squared summed over initial and final internal d.o.f. It is understood that $\{kl\} = \{lk\}$ and it appears in the sum only once. The symmetry factor $(1 + \delta_{kl})^{-1}$ is related to the exchange of identical particles in the final state. This formula incorporates annihilations, semi-annihilations and inelastic scatterings. Following [116] and [117], we treat the elastic scatterings in the Fokker-Planck approximation, effectively involving expansion in small momentum transfer.

Including also all possible decays of x_2 and H^\pm , and neglecting the quantum degeneracy effects in all the cases that we consider, such that $(1 \pm f) \approx 1$, the cBE system for the

i -th particle has the form:

$$\begin{aligned} \frac{Y'_i}{Y_i} = & -\frac{s}{x\tilde{H}} \frac{1}{Y_i} \left\{ \sum_{j\{kl\}} \left(Y_i Y_j I_{ij \rightarrow kl} - Y_k Y_l \frac{(1 + \delta_{ij})}{(1 + \delta_{kl})} I_{kl \rightarrow ij} \right) \right. \\ & \left. - \frac{m_j^2 T}{3\pi^2 s^2} K_1 \left(\frac{m_j}{T} \right) \left(\frac{Y_j}{Y_j^{\text{eq}}} - \frac{Y_i}{Y_i^{\text{eq}}} \right) \sum_{\{kl\}} \frac{\Gamma_{j \rightarrow ikl}}{(1 + \delta_{kl})} + (j \leftrightarrow i) \right\}, \end{aligned} \quad (4.8)$$

$$\begin{aligned} \frac{y'}{y} + \frac{Y'_{x_1}}{Y_{x_1}} = & -\frac{s}{x\tilde{H}} \frac{1}{Y_{x_1}} \sum_{j\{kl\}} \left(Y_{x_1} Y_j J_{x_1 j \rightarrow kl} - Y_k Y_l \frac{(1 + \delta_{x_1 j})}{(1 + \delta_{kl})} \frac{\sqrt{T_k T_l}}{T_{x_1}} K_{kl \rightarrow x_1 j} \right) \\ & + \frac{s}{x\tilde{H}} \frac{1}{Y_{x_1}} \sum_{j\{kl\}} Y_j \frac{D_{j \rightarrow ikl}}{(1 + \delta_{kl})} + \frac{\gamma(x)}{x\tilde{H}} \left(\frac{y^{\text{eq}}}{y} - 1 \right) \\ & + \frac{H}{x\tilde{H}} \frac{g_{x_1}}{3n_{x_1} T_{x_1}} \frac{Y_{x_1}}{Y_{x_1}^{\text{eq}}} \int \frac{d^3 p}{(2\pi)^3} \frac{\mathbf{p}^4}{E^3} f_{x_1}^{\text{eq}}(\mathbf{p}), \end{aligned} \quad (4.9)$$

where $\tilde{H} \equiv H/[1 + \tilde{g}(x)]$ and $\tilde{g} \equiv \frac{1}{3} \frac{T}{g_{\text{eff}}^s} \frac{dg_{\text{eff}}^s}{dT}$ with g_{eff}^s being the number of entropy degrees of freedom, the sum goes over all possible j states and $\{kl\}$ two-particle states, K_1 is the modified Bessel function of order 1, $\Gamma_{j \rightarrow ikl}$ stands for the decay width of the j -particle into ikl states and the rates are defined below.⁸ This is a set of 4 coupled ordinary differential equations that describe the evolution of comoving number densities of x_1 , x_2 and H^\pm , as well as the temperature of x_1 .

The evolution of the above system is governed by the interaction rates in the form of the momentum transfer rate $\gamma(x)$, as defined in [64], and integrals I, J, K defined as follows. The number-changing processes are described by the following integral⁹

$$I_{ij \rightarrow kl} = \frac{1}{n_i^{\text{eq}} n_j^{\text{eq}}} \int d\Pi_i d\Pi_j g_i g_j W_{ij \rightarrow kl} f_i^{\text{eq}}(T_i) f_j^{\text{eq}}(T_j), \quad (4.11)$$

through the use of the dimensionless invariant rate [119],

$$W_{ij \rightarrow kl}(s) \equiv \frac{1}{g_i g_j (1 + \delta_{kl})} \int d\Pi_k d\Pi_l (2\pi)^4 \delta^{(4)}(p_i + p_j - p_k - p_l) \left| \bar{M} \right|_{ij \leftrightarrow kl}^2 \quad (4.12)$$

⁸Note that there are no additional factors related to the number of particles being created or destroyed in a given process, as those come up automatically when one starts from the expression (4.7). In particular, for semi-annihilation one needs to sum over the processes in which the particle under consideration appears in the initial and in the final states, e.g., $ij \rightarrow \{kl\} = x_1 x_1 \rightarrow \{X_1 Z\}$ as well as $ij \rightarrow \{kl\} = x_1 Z \rightarrow \{X_1 X_1\}$. Accounting for the symmetry factor in the general collision term this leads to the well-known form of the Boltzmann equation, where the semi-annihilation term has a factor 1/2 compared to the annihilation term (see the notes inside ref. [118]).

⁹This is a generalization of the thermally averaged cross section for the case of (co-)(semi-)annihilating particles with different temperatures. Indeed, for $T_i = T_j \equiv T'$ this expression is the same as in ref. [119]. Following their evaluation one finds

$$I_{ij \rightarrow kl}(T') = \frac{1}{n_i^{\text{eq}} n_j^{\text{eq}}} \frac{T'}{32\pi^4} \int_{(m_i + m_j)^2}^{\infty} ds g_i g_j p_{ij} W_{ij \rightarrow kl} K_1 \left(\frac{\sqrt{s}}{T'} \right) = \langle \sigma v_{\text{Mol}} \rangle_{ij \rightarrow kl}, \quad (4.10)$$

where we used $p_{ij} = \sqrt{s - (m_i + m_j)^2} \sqrt{s - (m_i - m_j)^2} / (2\sqrt{s})$.

that is related to the cross section via $W_{ij \rightarrow kl} = 4p_{ij}\sqrt{s}\sigma_{ij}$. The integrals involved in the temperature evolution,

$$J_{ij \rightarrow kl} = \frac{1}{T_i n_i^{\text{eq}} n_j^{\text{eq}}} \int d\Pi_i d\Pi_j \frac{p_i^2}{3E_i} g_i g_j W_{ij \rightarrow kl} f_i^{\text{eq}}(T_i) f_j^{\text{eq}}(T_j), \quad (4.13)$$

$$K_{kl \rightarrow ij} = \frac{1}{\sqrt{T_k T_l} n_k^{\text{eq}} n_l^{\text{eq}}} \frac{1}{(1 + \delta_{ij})} \int d\Pi_i d\Pi_j d\Pi_k d\Pi_l (2\pi)^4 \delta^{(4)}(p_i + p_j - p_k - p_l) \frac{p_i^2}{3E_i} \times \left| \bar{M} \right|_{ij \leftrightarrow kl}^2 f_k^{\text{eq}}(T_k) f_l^{\text{eq}}(T_l), \quad (4.14)$$

$$D_{j \rightarrow ikl} = \frac{1}{3T_i n_j^{\text{eq}}} \int d\Pi_i d\Pi_j d\Pi_k d\Pi_l (2\pi)^4 \delta(p_i - p_j - p_k - p_l) \frac{p_i^2}{E_i} \left| \bar{M} \right|_{j \leftrightarrow ikl}^2 f_j^{\text{eq}}(T_j), \quad (4.15)$$

describe the change in energy due to forward processes (annihilations), backward processes (inverse annihilations) and decays, respectively.

Numerical solution of the above cBE system is relatively CPU expensive, in large part due to necessity of calculating a large number of rates.¹⁰ To render the task manageable, the numerical procedure we follow is to first determine for each of the parameter point if the full cBE system is needed or if the standard approach assuming kinetic equilibrium for the DM particle should suffice. For that we impose a rather conservative condition that if $\gamma(x)/H(x)|_{x=100} \geq 10$, then for the whole period of chemical freeze-out the elastic scatterings are assumed to be efficient enough to keep the DM in kinetic equilibrium, even in the presence of other disruptive processes like decay of a heavier dark sector state, and the assumption of $T_{x1} = T$ is well justified allowing for calculations using only the eq. (4.8). Conversely, if the scattering rate is smaller, $\gamma(x)/H(x)|_{x=100} < 10$, then the full cBE system is solved.

The needed rates were calculated using FeynCalc [120] for the matrix elements and using the DRAKE thermal average routines. On top of that the decay widths were utilized from the micrOMEGAs calculation. The latter was also used to include in the number density equation typically sub-dominant, but in some cases important annihilations to final states including virtual Z or W bosons, where we followed the procedure as described in the micrOMEGAs manual [114]. Heavier dark sector states were assumed to take part in co-annihilations and inelastic scattering processes if their mass did not exceed 50% of the DM state and the binary collision rates were truncated for processes that contribute less than 1% at the approximate time of freeze-out.

In figure 1 we show the thermal history of two example benchmark points for which kinetic decoupling happens early enough to have an impact on the final relic abundance. The left plot shows the evolution of the yield and how it differs between the cBE and the usual approach assuming kinetic equilibrium throughout (which we call nBE), while right plot highlights how the temperature evolution can differ from the one of the SM plasma. Both example points have strong semi-annihilation and kinetic decoupling happening at a time when the annihilations are still active, thus leading to a modification of the evolution of the DM number density.

¹⁰Note that in contrast to annihilation processes, the inelastic scatterings and semi-annihilations cannot be always included with the use of inclusive cross sections, but rather one has to perform the thermal average for every exclusive process separately.

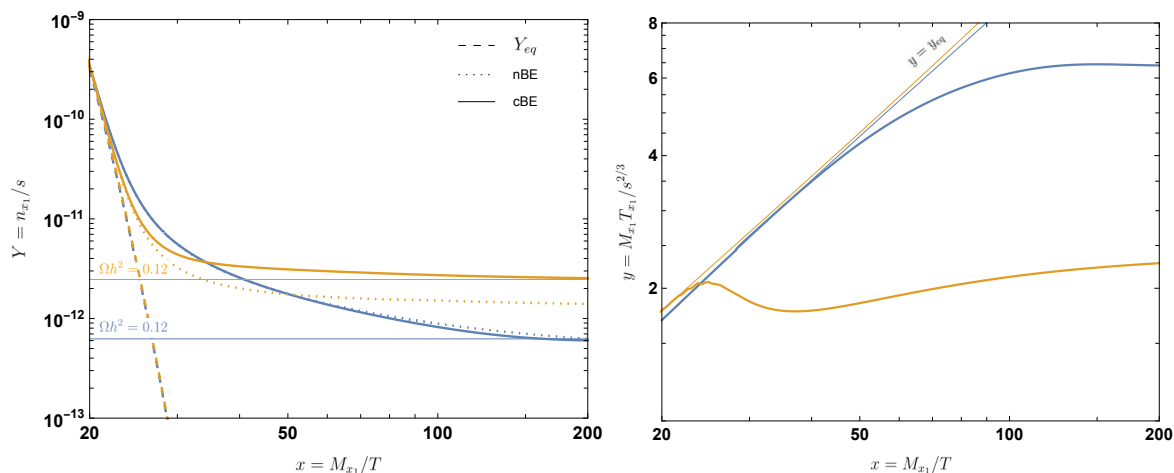


Figure 1. An example evolution of the yield Y (left) and the temperature parameter y (right) for two benchmark points with parameters: $M_{x_1} = 691.38$ GeV, $M_{x_2} = 1388.03$ GeV, $M_{H^+} = 1388.03$ GeV, $\sin \theta = 0.001264$, $\mu_S'' = 3943.34$ GeV, $\lambda_{S12} = \lambda_{S1} = \lambda_{S2} = 0$, $\lambda_S = \lambda_2 = \pi$, $\lambda_3 = 0$ (blue) and $M_{x_1} = 175.31$ GeV, $M_{x_2} = 264.34$ GeV, $M_{H^+} = 415.59$ GeV, $\sin \theta = 5.59 \times 10^{-4}$, $\mu_S'' = 859.79$ GeV, $\lambda_{S12} = 2.722$, $\lambda_{S1} = 2.5 \times 10^{-5}$, $\lambda_{S2} = 1.163$, $\lambda_S = \lambda_2 = \pi$, $\lambda_3 = 0.5759$ (orange). The solid lines give the actual thermal history as described by the cBE system, while dotted the nBE one.

5 Phase transition and gravitational waves

The vacuum in which we live today corresponds to the minimum of the scalar potential located at the broken EW phase $(h, H, s) = (v, 0, 0)$. In the first moments of the Universe, however, the temperature was so large that thermal corrections influenced the $T = 0$ effective potential significantly. As one goes back in time, the temperature rises and the increasing thermal effects push the low-temperature minimum (or true vacuum) upward: it becomes higher than the minimum at the origin and eventually disappears. Thus in the limit of $T \rightarrow \infty$, the high-temperature, symmetric phase is usually $(h, H, s) = (0, 0, 0)$; the symmetry is restored. A more complicated possibility is symmetry non-restoration, where in this limit the minimum of the potential does not go to the origin [121, 122], or inverse symmetry breaking [123], where a symmetry, not broken at low temperature, is broken at high temperature.

In our case, the story thus begins at the origin of the potential, in the high-temperature phase. Then as the temperature decreases, the potential develops a second minimum, say along the h axis, where the potential is initially larger than at the origin. With time, the temperature continues to decrease until these two phases become degenerate: the value of the potential in both vacua is identical. The temperature at which it occurs is the critical temperature T_c . At some lower temperature, the field will eventually tunnel from this false vacuum to a deeper stable minimum (or true vacuum), here along the h axis. This tunneling occurs through the nucleation of bubbles of true vacuum, which expand and collide with each other, filling the Universe little by little and thereby gradually converting the false vacuum into the true vacuum. The collision between these bubbles is responsible for the generation of a stochastic gravitational-wave background. The temperature at which one bubble nucleates per Hubble volume is called the nucleation temperature T_n . For a fast

first-order phase transition without large reheating, this can be considered as the temperature at which gravitational waves are produced [124].¹¹ Finally, the value of the Higgs VEV smoothly evolves towards its tree-level value v as the temperature approaches zero.

A couple of important parameters capture the most information about a first-order phase transition. The strength of a first-order phase transition is characterized by the vacuum energy $\Delta\epsilon$ released during the phase transition. To obtain a dimensionless parameter α , one normalizes this vacuum energy to the energy density of the plasma outside the bubbles ρ_{rad} [126]:

$$\alpha \equiv \frac{\Delta\epsilon}{\rho_{\text{rad}}}\Big|_{T=T_*}, \quad \Delta\epsilon \equiv \epsilon|_{\text{false vacuum}} - \epsilon|_{\text{true vacuum}} \quad (5.1)$$

with $\epsilon = V_{\text{eff}} - \frac{T}{4} \frac{\partial V_{\text{eff}}}{\partial T}$, T_* the temperature at which GWs are generated and $\rho_{\text{rad}} = \frac{\pi^2}{30} g_* T^4$, where g_* is the effective number of relativistic degrees of freedom at the temperature T . Note that a first-order phase transition is characterized as a strong one if the ratio of the VEV to the temperature, evaluated at T_* , satisfies

$$\frac{v_*}{T_*} \geq 1. \quad (5.2)$$

If this ratio is much smaller than unity the nature of the PT cannot be distinguished without lattice calculations, as also evidenced by the numerically very small value of the would-be GW signal in this case [69, 127, 128]. The inverse time duration of the PT, β , is usually normalized by the Hubble parameter $H_* \equiv H(T_*)$ [129]:

$$\frac{\beta}{H_*} = T \frac{d(S/T)}{dT}\Big|_{T=T_*}, \quad (5.3)$$

where $S \equiv S(h, H, s, T)$ is the 3-dimensional Euclidean action computed for an $O(3)$ -symmetric critical bubble. A large β/H_* means that we can safely neglect the Hubble expansion of the Universe during the phase-transition process.

A single bubble cannot generate gravitational waves, because its quadrupole moment vanishes due of its spherical symmetry. The key ingredient for a stochastic GW background to be generated is the collisions between these bubbles of true vacuum, as mentioned above. Indeed, this will break the spherical symmetry of each of the collided scalar-field bubbles [130]. For bubbles evolving in a thermal plasma, additional contributions to the GW signal come from the metric perturbation induced by the plasma: sound waves [131, 132] and magnetohydrodynamic (MHD) turbulence [133]. Sub- and supersonic bubbles, respectively, create compression waves beyond the bubble wall and rarefaction waves behind it. When acoustic waves from different bubbles overlap, the induced shear stress of the metric generate gravitational waves. Finally, bubble collision is responsible for the turbulent motion of the fully ionized plasma. These MHD turbulences will generate gravitational waves. The power spectrum $h^2\Omega_{\text{GW}}$ of the stochastic GW background from a cosmic phase transitions thus arises from three contributions [124]: $h^2\Omega_{\text{GW}} \simeq h^2\Omega_{\text{col}} + h^2\Omega_{\text{sw}} + h^2\Omega_{\text{turb}}$.¹² Note that the treatment of cosmic phase transitions suffers from uncertainties due to gauge or

¹¹See. ref. [125] for a discussion of subtleties.

¹²In situations of strong supercooling, the GW power spectrum from sound-waves becomes similar to the contribution from bubble collision [134].

renormalisation-scale dependence for instance, that could potentially lower the resulting GW signal strength [135, 136].

The scalar-field contribution redshifted to today is given in the envelope approximation by [137]¹³

$$h^2\Omega_{\text{col}}(f) = h^2\Omega_{\text{col}}^{\text{peak}} S_{\text{col}}(f), \quad (5.4)$$

with

$$h^2\Omega_{\text{col}}^{\text{peak}} = 1.67 \times 10^{-5} \left(\frac{H_*}{\beta}\right)^2 \left(\frac{\kappa_{\text{col}}\alpha}{1+\alpha}\right)^2 \left(\frac{100}{g_*}\right)^{1/3} \left(\frac{0.11v_w^3}{0.42+v_w^2}\right), \quad (5.5)$$

$$S_{\text{col}} = \frac{3.8 (f/f_{\text{col}})^{2.8}}{1 + 2.8 (f/f_{\text{col}})^{3.8}},$$

where κ_{col} is the efficiency factor for the conversion of the vacuum energy into the gradient energy of the scalar field (energy stored in the shell of the scalar-field bubbles), v_w is the bubble-wall speed in the rest frame of the plasma far away from the bubble [124] and f_{col} is the peak frequency, thus the frequency at $h^2\Omega_{\text{col}}^{\text{peak}}$.

The sound-wave contribution is given by [141–143]

$$h^2\Omega_{\text{sw}}(f) = h^2\Omega_{\text{sw}}^{\text{peak}} S_{\text{sw}}(f), \quad (5.6)$$

with¹⁴

$$h^2\Omega_{\text{sw}}^{\text{peak}} = 1.23 \times 10^{-6} \left(\frac{H_*}{\beta}\right) \left(\frac{\kappa_{\text{sw}}\alpha}{1+\alpha}\right)^2 \left(\frac{100}{g_*}\right)^{1/3} v_w \Upsilon, \quad (5.7)$$

$$S_{\text{sw}} = \left(\frac{f}{f_{\text{sw}}}\right)^3 \left(\frac{7}{4 + 3(f/f_{\text{sw}})^2}\right)^{7/2},$$

where κ_{sw} is the efficiency factor for the conversion of the vacuum energy into the bulk motion of the plasma and f_{sw} is the sound-wave peak frequency. The suppression factor for a radiation-dominated Universe is defined as [144, 145]

$$\Upsilon = 1 - \frac{1}{\sqrt{2\tau_{\text{sw}}H + 1}}, \quad (5.8)$$

where τ_{sw} is the time after which sound waves do not source the GW production and where $\Upsilon \simeq \tau_{\text{sw}}H$ when $\tau_{\text{sw}}H \ll 1$, thus when this time is much smaller than a Hubble time.

Finally, the MHD-turbulence contribution is given by [124, 146]

$$h^2\Omega_{\text{turb}}(f) = h^2\Omega_{\text{turb}}^{\text{peak}} S_{\text{turb}}(f), \quad (5.9)$$

with

$$h^2\Omega_{\text{turb}}^{\text{peak}} = 3.35 \times 10^{-4} \left(\frac{H_*}{\beta}\right) \left(\frac{\kappa_{\text{turb}}\alpha}{1+\alpha}\right)^{3/2} \left(\frac{100}{g_*}\right)^{1/3} v_w \left[\frac{1}{2^{11/3} (1 + 8\pi f_{\text{turb}}/h_*)}\right], \quad (5.10)$$

$$S_{\text{turb}} = \frac{(f/f_{\text{turb}})^3}{[1 + (f/f_{\text{turb}})]^{11/3}} \left[\frac{2^{11/3} (1 + 8\pi f_{\text{turb}}/h_*)}{1 + 8\pi f/h_*}\right], \quad (5.11)$$

¹³Recent works on contribution from bubble collisions can be found in [134, 138–140].

¹⁴The derivation of this ready-to-use formula is given in appendix C.

where κ_{turb} is the efficiency factor for the conversion of the vacuum energy into the MHD turbulences, f_{turb} is the MHD-turbulence peak frequency and h_* is the today-redshifted value of the Hubble rate at T_* .

6 Numerical scan

We used Markov Chain Monte Carlo (MCMC) with the Metropolis-Hastings algorithm in order to generate points, starting with a number of points with the DM relic density within the Planck 3σ range. We then imposed other constraints: perturbativity, perturbative unitarity, bounded-from-below conditions for the scalar potential, globality of the EW vacuum, bounds on electroweak precision parameters S , T and U , Higgs invisible width and Higgs to diphoton $h \rightarrow \gamma\gamma$ decay.

We performed three scans:

1. Points with non-zero quartic λ_{S12} coupling (and $\mu_S'' = \lambda_{S1} = \lambda_{S2} = \lambda_3 = 0$)
2. Points with non-zero cubic μ_S'' coupling (and $\lambda_{S12} = \lambda_{S1} = \lambda_{S2} = \lambda_3 = 0$)
3. General points with non-zero μ_S'' and λ_{S12} and without conditions on the quartic portals λ_{S1} , λ_{S2} , λ_3 .

In the first two cases, all the biquadratic portal couplings were set to zero, i.e. $\lambda_{S1} = \lambda_{S2} = \lambda_3 = 0$, except for λ_4 , because this would have entailed enforcing a special relation between M_{x_2} and M_{H^\pm} . Since we need a non-zero mixing angle θ between x_1 and x_2 , the μ_{SH} mixing term was non-zero in all cases. The dark sector scalar self-couplings were set to $\lambda_S = \lambda_2 = \pi$ in order to allow for larger values of λ_{S12} and μ_S'' which are otherwise constrained by vacuum stability.

New points were generated from a multivariate normal distribution. The initial covariance matrix was calculated from a set of a few tens of points with DM relic density within the Planck 3σ bounds. The initial values for M_{x_2} and M_{H^\pm} were chosen in an interval around $2M_{x_1}$ in order to enhance semi-annihilation processes. The covariance matrix was updated with each added point, while its norm was kept constant to ensure a reasonable acceptance ratio of points. Dimensionful quantities M_{x_1} , M_{x_2} , M_{H^\pm} and μ_S'' were generated logarithmically and only points with $M_{x_1} < M_{x_2}, M_{H^\pm}$ kept. Similarly to the calculation of the initial distribution, a few tens of points with DM relic density within the Planck 3σ bounds and varied couplings were used to start the MCMC chains from a few hundred up to thousand points in length. Since the desired probability distributions of our MCMCs were rather arbitrary, we do not consider the density of points in our plots to have a specific statistical meaning.

The desired distribution for each case consists of a product of Gaussians whose central values and standard deviations are given in table 1. Extra suppression factors of an arbitrary small value 10^{-12} were used to make the Gaussians essentially one-sided when the conditions $\sin \theta > 0$ and $0 \leq \lambda_{S12} < 4$ (the maximal value from vacuum stability bounds for $\lambda_S = \lambda_2 = \pi$ and portal couplings $\lambda_{S1} = \lambda_{S2} = \lambda_3 = 0$), and $1 \leq \mu_S''/\text{GeV} < 2\sqrt{\lambda_S}M_{x_1}/\text{GeV}$ did not hold true. In the last condition, used in the second and third scans, we limited the cubic coupling by $|\mu_S''| < 2\sqrt{\lambda_S}M_{x_1}$, the bound from absolute vacuum stability in the \mathbb{Z}_3 singlet limit.

Quantity	Central value	Standard deviation
$\Omega_c h^2$	0.120	0.001
M_{x_1}/GeV	333.33	500
M_{x_2}/GeV	$2M_{x_1}/\text{GeV}$	250
M_{H^\pm}/GeV	$2M_{x_1}/\text{GeV}$	250
$\sin \theta$	0	0.125
$ M_{x_2} - M_{H^\pm} /\text{GeV}$	0	360
μ_S''/GeV	$2\sqrt{\lambda_S}M_{x_1}/\text{GeV}$	$\frac{1}{3} \times 2\sqrt{\lambda_S}M_{x_1}/\text{GeV}$

Table 1. The central values and standard deviations for the desired distribution of the MCMC.

Notice that unlike in the singlet-only limit, the cubic μ_S'' coupling can yield semi-annihilation together with the ever-present mixing term μ_{SH} .

7 Signals

We now discuss the results of the scan, in particular for the direct-detection and gravitational-wave signals.

7.1 Direct detection

In figure 2 we show the predictions for the spin-independent direct detection cross section for the three cases. The top panel shows points with non-zero λ_{512} , the middle panel points dominated by μ_S'' and the bottom panel shows the points from the more general scan. Also shown are the sensitivity curves of the XENON1T (2018) [11], PandaX-4T (2021) [12], LZ (2022) [13] in grey and the projected sensitivity curve for XENONnT [147] in dashed grey. The color code shows the semi-annihilation fraction r defined by

$$r = \frac{1}{2} \frac{v\sigma_{xx \rightarrow x^*X}}{v\sigma_{xx^* \rightarrow XX} + \frac{1}{2}\sigma_{xx \rightarrow x^*X}}, \quad (7.1)$$

where x denotes x_1, x_2, H^\pm and X stands for any SM particles. With dominant semi-annihilation r approaches unity. The points with early kinetic decoupling, evaluated with the cBE method detailed in section 4, are marked with crosses.

7.2 Gravitational waves

For each of the three scans mentioned in section 6, we study how the Universe ends in the EW vacuum $(v, 0, 0)$ at zero temperature. If at least one phase transition, to reach that state, is of the first order, then we subsequently compute the power spectrum of the stochastic GW background $h^2\Omega_{\text{GW}}$, necessarily associated to these cosmic FOPTs. In addition to the previous constraints, we also take into account the constraint from direct-detection experiments: only points not excluded by LZ are displayed in figure 3 and figure 4. Note also that we consider a relativistic bubble-wall speed, $v_w = 1$.

In the left panel of figure 3, we show, for the three scans, the region of the parameter space, projected onto the plane made by the mixing angle $\sin \theta$ and the DM mass M_{x_1} , that gives rise to first-order phase transitions. These are essentially obtained for large mixing and

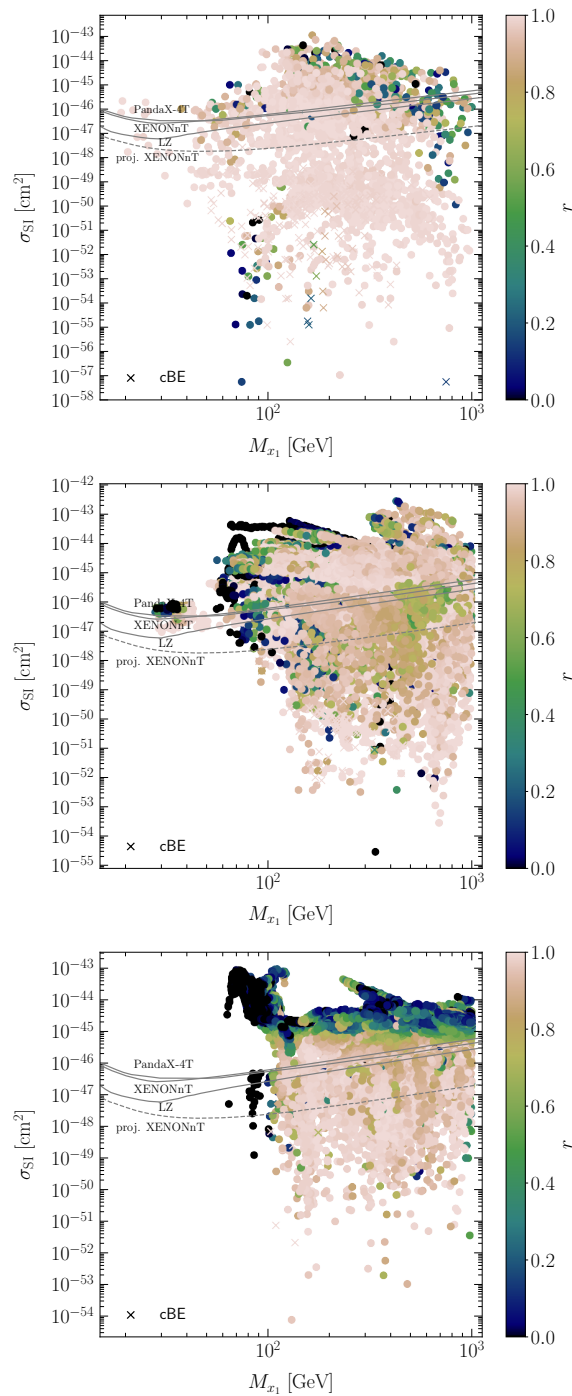


Figure 2. Spin-independent direct detection cross section vs. dark matter mass. Top panel: points dominated by λ_{S12} ; middle panel: points dominated by μ'_S and μ_{SH} ; bottom panel: more general points. Also shown are the sensitivity curves of the XENON1T (2018) [11], PandaX-4T (2021) [12], LZ (2022) [13] in grey and the projected sensitivity curve for XENONnT [147] in dashed grey.

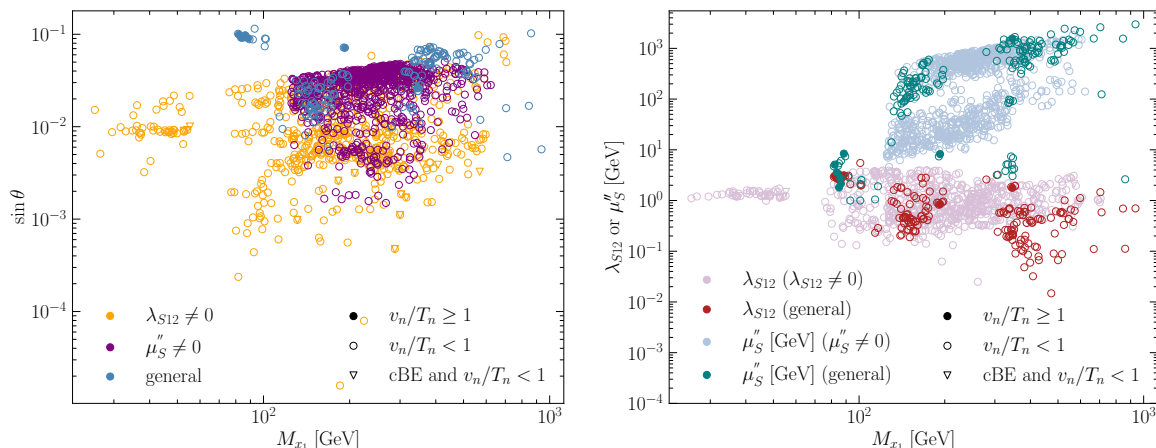


Figure 3. Projection of the parameter space, showing points which satisfy all the theoretical/experimental constraints. cBE points that lead to FOPT are only found for $\lambda_{S12} \neq 0$ scan. Strong FOPT are only found for general scan. Left panel: Sine of the mixing angle $\sin \theta$ vs. DM mass M_{x_1} . Right panel: λ_{S12} vs. M_{x_1} for both the $\lambda_{S12} \neq 0$ and general scan and μ_S'' vs. M_{x_1} for both the $\mu_S'' \neq 0$ and general scan.

mild to large DM mass. We see that only points from the general scan lead to strong FOPTs. The right panel shows the values of either λ_{S12} or μ_S'' , as a function of M_{x_1} , responsible for FOPTs for scans where they are non-zero. In both panels, triangles are points for which the cBE method has been used to compute the DM relic density, as the scattering rate is not sufficient to consider kinetic equilibrium for DM during the freeze-out process (see section 4).

The signal from the stochastic gravitational-wave background is shown in figure 4, with the power-law integrated (PLI) sensitivity curves of LISA, DECIGO and BBO, obtained for an observation time of 4 years and a threshold value for the signal-to-noise ratio to be 10 [148, 149]. Similarly to figure 2, we show the semi-annihilation fraction with a color code. The upper panel of figure 4 shows the GW signal for the scan with non-zero λ_{S12} . This signal results from single-step FOPTs. We can see that none of the points leads to strong FOPTs and that for some of them (triangles), the assumption of kinetic equilibrium does not hold and the full cBE system should be solved. The middle panel shows the GW signal for the scan with non-zero μ_S'' . Again, we only find single-step weak FOPTs. A cubic term helps to generate a barrier in the potential and thus enhance the strength of the phase transition. However, we only find a single-step FOPT from the origin towards the EW minimum, thereby along the Higgs direction h . This is why a non-zero μ_S'' is not helpful here to obtain a stronger PT, as it only impacts the s direction. Finally, the lower panel of figure 4 shows the GW signal for the general scan, where strong FOPTs are obtained and where one of the points clearly lies above the LISA PLI sensitivity curve, thus yielding a detectable GW signal. Note that we also found two-step phase transitions. For each of them, indicated by a triangle, the first step $(0, 0, 0) \rightarrow (0, v_H, 0)$ is a second-order PT and is followed by a first-order PT $(0, v_H', 0) \rightarrow (v_h, 0, 0)$. Note also that from figure 4, it seems that the lower the semi-annihilation fraction, the stronger the GW signal. However, if we do not take experimental constraints into account, the correlation between the strength of the GW signal and the semi-annihilation fraction is lost.

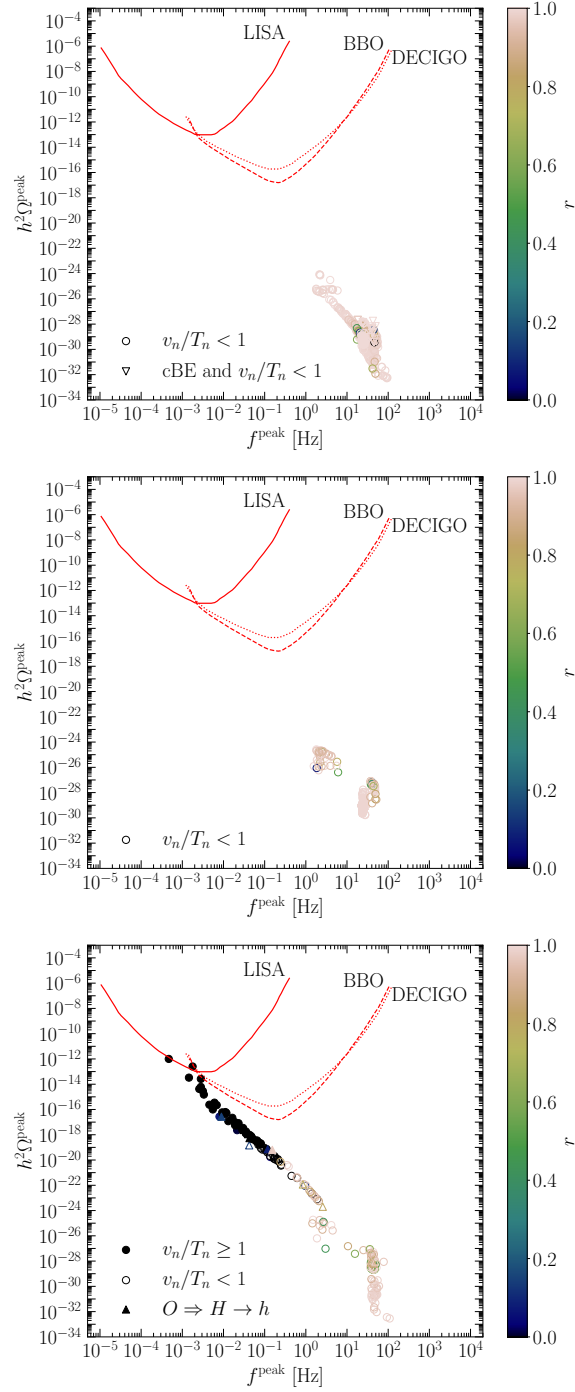


Figure 4. Peak amplitude of the GW signal as a function of peak frequency. The top panel shows points with non-zero λ_{S12} , the middle panel points dominated by μ_S'' and the bottom panel shows the points from the more general scan. Also shown are the PLI sensitivity curves of future detectors LISA, BBO and DECIGO.

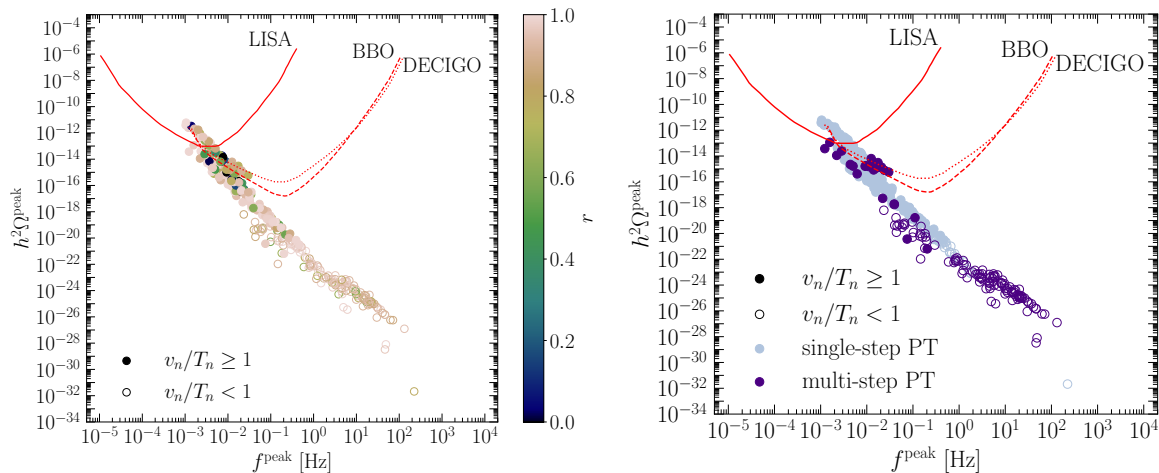


Figure 5. Peak amplitude of the GW signal as a function of peak frequency with points from the scan in eq. (7.2). Also shown are the PLI sensitivity curves of future detectors LISA, BBO and DECIGO. The left panel highlights the semi-annihilation rate, while the right panel distinguishes single-step from multi-step PTs.

Finally, let us stress that in principle, in this model, if we relax the constraint on relic density and allow for underabundant DM, we can more easily find regions of the parameter space allowing for different kind of multi-step phase transitions in the three-dimensional field space (h, H, s) and/or leading to a strong enough GW signal to be detected by LISA, DECIGO or BBO, as can be seen in figure 5. The points in this figure comply with all the theoretical/experimental constraints, except that they only lead to underabundant DM, and result from a random scan in the following range:

$$\begin{aligned}
 M_{x_1} \in [10, 1000] \text{ GeV}, & & M_{x_2}, M_{H^\pm} \in [M_{x_1}, 1000 \text{ GeV}], & & \sin \theta \in [0, \sqrt{2}/2], \\
 \mu_S'' \in [0, 2000] \text{ GeV}, & & \lambda_3, \lambda_{S1}, \lambda_{S2}, \lambda_{S12} \in [-4\pi, 4\pi], & & \lambda_2, \lambda_S \in [-\pi, 4\pi].
 \end{aligned} \quad (7.2)$$

8 Conclusions

We have explored the cosmology of the \mathbb{Z}_3 symmetric dark matter model with an inert doublet and a complex singlet with the emphasis on detectability of the gravitational-wave signal and dark-matter phenomenology. In order for the model to be in agreement with direct-detection limits the dark matter candidate needs to be a singlet-like state arising from the mixing of the singlet and the neutral part of the inert doublet. This setup opens an interesting possibility of important or even dominant semi-annihilation processes that modifies the thermal DM production through an early kinetic decoupling: if the relic density is determined via semi-annihilation, the dark matter-Higgs boson couplings that would keep DM in kinetic equilibrium via elastic collisions are suppressed.

We performed MCMC scans to not only produce general coupling configurations available to the model, but also to look specifically at large semi-annihilation (through a large cubic coupling μ_S'' or the quartic semi-annihilation coupling λ_{S12} coupling). We find that for the

points with dominant semi-annihilation, strong suppression of the direct-detection signal comes also with weak FOPTs whose GW signals would lie orders of magnitude below detection projections in a foreseeable future. On the other hand, a general scan of the model reveals points near the detection limits of LISA, DECIGO and BBO.

We then also computed the GW signal for uniformly distributed random general scan allowing for underabundant singlet-like x_1 with relic density below the Planck constraint. (There could be either an additional non-thermal production mechanism or another DM component.) In that case we found a sizable portion of the parameter space leading to a single-step or a multi-step phase transition producing strong enough GW signal to be potentially detected by LISA, DECIGO or BBO.

Therefore, we conclude that in the \mathbb{Z}_3 symmetric model with an inert doublet and a complex singlet there exists a parameter range that explaining whole dark matter *and* providing potentially observable GW peak amplitude, though it is rather small and challenging to be observed in the near future. Nevertheless, when extending the analysis to underabundant dark matter the detection prospects of the GW peak amplitude become significantly more promising.

Acknowledgments

This work was supported by the Estonian Research Council grants PRG434, PRG803, RVTT3 and RVTT7, and by the CoE program TK202 ‘‘Fundamental Universe’’. The work of A.H. was supported by the National Science Centre, Poland, research grant No. 2021/42/E/ST2/00009. The work of M.L. is supported by the National Science Centre, Poland, research grant No. 2020/38/E/ST2/00243.

A Field-dependent scalar mass matrices

The field-dependent scalar masses $m_i^2 \equiv m_i^2(h, H, s)$, present in eq. (2.6) and eq. (2.10), correspond to the eigenvalues of the field-dependent mass matrices of the scalar fields M_S^2 , of the pseudoscalar fields M_P^2 and of the charged fields M_C^2 :

$$M_S^2 = \begin{pmatrix} \mu_1^2 + 3\lambda_1 h^2 + \frac{\lambda_3 + \lambda_4}{2} H^2 + \frac{\lambda_{S1}}{2} s^2 & (\lambda_3 + \lambda_4)hH + \frac{\lambda_{S12s} + \sqrt{2}\mu_{SH}}{4} s & \lambda_{S1}hs + \frac{\lambda_{S12}}{2} Hs + \frac{\sqrt{2}\mu_{SH}}{4} H \\ (\lambda_3 + \lambda_4)hH + \frac{\lambda_{S12s} + \sqrt{2}\mu_{SH}}{4} s & \mu_2^2 + 3\lambda_2 H^2 + \frac{\lambda_3 + \lambda_4}{2} h^2 + \frac{\lambda_{S2}}{2} s^2 & \lambda_{S2}Hs + \frac{\lambda_{S12}}{2} hs + \frac{\sqrt{2}\mu_{SH}}{4} h \\ \lambda_{S1}hs + \frac{\lambda_{S12}}{2} Hs + \frac{\sqrt{2}\mu_{SH}}{4} H & \lambda_{S2}Hs + \frac{\lambda_{S12}}{2} hs + \frac{\sqrt{2}\mu_{SH}}{4} h & \mu_S^2 + 3\lambda_S s^2 + \frac{3}{\sqrt{2}}\mu_S'' s \\ & & + \frac{\lambda_{S1}h^2 + \lambda_{S2}H^2 + \lambda_{S12}hH}{2} \end{pmatrix}, \quad (\text{A.1})$$

$$M_P^2 = \begin{pmatrix} \mu_1^2 + \lambda_1 h^2 + \frac{\lambda_3 + \lambda_4}{2} H^2 + \frac{\lambda_{S1}}{2} s^2 & \frac{\lambda_{S12s} + \sqrt{2}\mu_{SH}}{4} s & \frac{\lambda_{S12}}{2} Hs - \frac{\sqrt{2}\mu_{SH}}{4} H \\ \frac{\lambda_{S12s} + \sqrt{2}\mu_{SH}}{4} s & \mu_2^2 + \lambda_2 H^2 + \frac{\lambda_3 + \lambda_4}{2} h^2 + \frac{\lambda_{S2}}{2} s^2 & -\frac{\lambda_{S12}}{2} hs + \frac{\sqrt{2}\mu_{SH}}{4} h \\ \frac{\lambda_{S12}}{2} Hs - \frac{\sqrt{2}\mu_{SH}}{4} H & -\frac{\lambda_{S12}}{2} hs + \frac{\sqrt{2}\mu_{SH}}{4} h & \mu_S^2 + \lambda_S s^2 - \frac{3}{\sqrt{2}}\mu_S'' s \\ & & + \frac{\lambda_{S1}h^2 + \lambda_{S2}H^2 - \lambda_{S12}hH}{2} \end{pmatrix}, \quad (\text{A.2})$$

$$M_C^2 = \begin{pmatrix} \mu_1^2 + \lambda_1 h^2 + \frac{\lambda_3}{2} H^2 + \frac{\lambda_{S1}}{2} s^2 & \frac{\lambda_4}{2} hH + \frac{\lambda_{S12s} + \sqrt{2}\mu_{SH}}{4} s \\ \frac{\lambda_4}{2} hH + \frac{\lambda_{S12s} + \sqrt{2}\mu_{SH}}{4} s & \mu_2^2 + \lambda_2 H^2 + \frac{\lambda_3}{2} h^2 + \frac{\lambda_{S2}}{2} s^2 \end{pmatrix}. \quad (\text{A.3})$$

Evaluated in the EW vacuum $(h, H, s) = (v, 0, 0)$, these mass matrices become

$$M_S^2 = \begin{pmatrix} \mu_1^2 + 3\lambda_1 v^2 & 0 & 0 \\ 0 & \mu_2^2 + \frac{\lambda_3 + \lambda_4}{2} v^2 & \frac{\sqrt{2}\mu_{SH}}{4} v \\ 0 & \frac{\sqrt{2}\mu_{SH}}{4} v & \mu_S^2 + \frac{\lambda_{S1} v^2}{2} \end{pmatrix}, \quad (\text{A.4})$$

$$M_P^2 = \begin{pmatrix} \mu_1^2 + \lambda_1 v^2 & 0 & 0 \\ 0 & \mu_2^2 + \frac{\lambda_3 + \lambda_4}{2} v^2 & \frac{\sqrt{2}\mu_{SH}}{4} v \\ 0 & \frac{\sqrt{2}\mu_{SH}}{4} v & \mu_S^2 + \frac{\lambda_{S1} v^2}{2} \end{pmatrix}, \quad (\text{A.5})$$

$$M_C^2 = \begin{pmatrix} \mu_1^2 + \lambda_1 h^2 & 0 \\ 0 & \mu_2^2 + \frac{\lambda_3}{2} v^2 \end{pmatrix}, \quad (\text{A.6})$$

thus putting in evidence the mixing between H_2 and S .

B Counter-terms

We present expressions for counter-terms in the effective potential used to keep VEVs, masses and mixing at their tree-level values. Since the counter-terms $\delta\lambda_3$ and $\delta\lambda_4$ only appear as a sum in eq. (2.8), we can arbitrarily set $\delta\lambda_4$ to zero. The counter-terms, expressed via derivatives of the one-loop Coleman-Weinberg potential (2.6), are given by

$$\delta\mu_1^2 = \frac{v\partial_h^2 \Delta V - 3\partial_h \Delta V}{4v}, \quad (\text{B.1})$$

$$\delta\mu_2^2 = \frac{v\partial_h \partial_{H^0}^2 V - 2\partial_{H^0}^2 \Delta V}{4}, \quad (\text{B.2})$$

$$\delta\mu_S^2 = \frac{v\partial_h \partial_{s_R}^2 V - 2\partial_{s_R}^2 \Delta V}{4}, \quad (\text{B.3})$$

$$\delta\mu_{SH} = -\partial_{H^0} \partial_{s_R} \Delta V, \quad (\text{B.4})$$

$$\delta\mu_S'' = -\frac{1}{6} \partial_{s_R}^3 \Delta V, \quad (\text{B.5})$$

$$\delta\lambda_1 = \frac{\partial_h \Delta V - v\partial_h^2 \Delta V}{8v^3}, \quad (\text{B.6})$$

$$\delta\lambda_3 = -\frac{1}{4v} \partial_h \partial_{H^0}^2 \Delta V, \quad (\text{B.7})$$

$$\delta\lambda_{S1} = -\frac{1}{4v} \partial_h \partial_{s_R}^2 \Delta V, \quad (\text{B.8})$$

$$\delta\lambda_{S12} = -\frac{1}{2v} \partial_{H^0} \partial_{s_R}^2 \Delta V. \quad (\text{B.9})$$

C Sound-wave contribution $h^2 \Omega_{\text{sw}}(f)$

From [141–143] one has¹⁵

$$h^2 \Omega_{\text{sw}}^{\text{peak}} = 3h^2 \times 0.687 F_{\text{gw},0} \Gamma^2 \bar{U}_f^4 \frac{H_* R_*}{c_s} \tilde{\Omega}_{\text{gw}} \Upsilon, \quad (\text{C.1})$$

¹⁵Note that in [142] the factor 3 is missing in eq. (C.1) and the factor $1/c_s$ is not considered in [141, 143].

where the mean adiabatic index $\Gamma = 4/3$ for a relativistic fluid, and the enthalpy-weighted root-mean-square of the fluid velocity \bar{U}_f is expressed as [143]:

$$\bar{U}_f = \sqrt{\frac{K}{\Gamma}}, \quad K = \frac{\kappa_{\text{sw}}\alpha}{1+\alpha}. \quad (\text{C.2})$$

The mean bubble separation at percolation temperature¹⁶ R_* is defined as

$$R_* = \frac{(8\pi)^{1/3} \max\{c_s, v_w\}}{\beta} \quad (\text{C.3})$$

with $c_s = 1/\sqrt{3}$ the speed of sound in the plasma [126].

The parameter $\tilde{\Omega}_{\text{gw}}$, which quantifies how efficiently the kinetic energy is converted into gravitational waves, is numerically found to be $\tilde{\Omega}_{\text{gw}} \simeq 1.2 \times 10^{-2}$ [141, 143].

Finally, the factor $F_{\text{gw},0}$ needed to obtain the today value $h^2\Omega_{\text{sw}}^{\text{peak}}$ is defined as [142, 143]

$$F_{\text{gw},0} = \Omega_{\gamma,0} \left(\frac{g_{s0}}{g_{s*}} \right)^{4/3} \frac{g_*}{g_0}, \quad (\text{C.4})$$

where $\Omega_{\gamma,0} \equiv \rho_{\gamma,0}/\rho_{c,0}$ is the photon density today, g_{s*} the effective number of entropic degrees of freedom, g_* the effective number of relativistic degrees of freedom, while g_{s0} and g_0 give their present values, respectively. The degrees of freedom g_{s*} and g_* are equal at the EW scale, while g_{s0} and g_0 are different since they are considered after the neutrino decoupling.

The following values for the aforementioned parameters allows us to compute the factor $F_{\text{gw},0}$ [150, 151]:

$$\begin{aligned} \rho_{\gamma,0} &= 0.26 \frac{\text{eV}}{\text{cm}^3}, & \rho_{c,0} &= 1.05 \times 10^{-5} h^2 \text{ GeV cm}^{-3}, & h &\equiv \frac{H_0}{100 \text{ km s}^{-1} \text{ Mpc}^{-1}}, \\ g_{s0} &\simeq 3.94 & \text{and } g_0 &\simeq 3.38, \end{aligned} \quad (\text{C.5})$$

where $N_{\text{eff}} = 3.044$ [152] has been used in the computation of g_{s0} and g_0 . Note that $g_{s0} \simeq 3.91$ and $g_0 = 2$ are considered in refs. [141, 142]. Considering these values, we can thus express $F_{\text{gw},0}$ as

$$F_{\text{gw},0} = \frac{9.77 \times 10^{-6}}{h^2} \left(\frac{100}{g_*} \right)^{1/3} \quad (\text{C.6})$$

Putting all together, we finally obtain

$$\begin{aligned} h^2\Omega_{\text{sw}}^{\text{peak}} &= 2.061 h^2 \frac{9.77 \times 10^{-6}}{h^2} \left(\frac{100}{g_*} \right)^{1/3} \left(\frac{\kappa_{\text{sw}}\alpha}{1+\alpha} \right)^2 \frac{H_* (8\pi)^{1/3} \max\{c_s, v_w\}}{\beta/\sqrt{3}} 1.2 \times 10^{-2} \Upsilon \\ &\simeq 1.23 \times 10^{-6} \left(\frac{H_*}{\beta} \right) \left(\frac{\kappa_{\text{sw}}\alpha}{1+\alpha} \right)^2 \left(\frac{100}{g_*} \right)^{1/3} \max\{c_s, v_w\} \Upsilon. \end{aligned} \quad (\text{C.7})$$

Open Access. This article is distributed under the terms of the Creative Commons Attribution License ([CC-BY4.0](https://creativecommons.org/licenses/by/4.0/)), which permits any use, distribution and reproduction in any medium, provided the original author(s) and source are credited.

¹⁶Here we consider that the nucleation and percolation temperature are very close to each other: $T_n \simeq T_p$.

References

- [1] PLANCK collaboration, *Planck 2018 results. VI. Cosmological parameters*, *Astron. Astrophys.* **641** (2020) A6 [*Erratum ibid.* **652** (2021) C4] [[arXiv:1807.06209](#)] [[INSPIRE](#)].
- [2] CMS collaboration, *Observation of a new boson at a mass of 125 GeV with the CMS experiment at the LHC*, *Phys. Lett. B* **716** (2012) 30 [[arXiv:1207.7235](#)] [[INSPIRE](#)].
- [3] ATLAS collaboration, *Observation of a new particle in the search for the Standard Model Higgs boson with the ATLAS detector at the LHC*, *Phys. Lett. B* **716** (2012) 1 [[arXiv:1207.7214](#)] [[INSPIRE](#)].
- [4] E. Ma, *Verifiable radiative seesaw mechanism of neutrino mass and dark matter*, *Phys. Rev. D* **73** (2006) 077301 [[hep-ph/0601225](#)] [[INSPIRE](#)].
- [5] L. Lopez Honorez, E. Nezri, J.F. Oliver and M.H.G. Tytgat, *The inert doublet model: an archetype for dark matter*, *JCAP* **02** (2007) 028 [[hep-ph/0612275](#)] [[INSPIRE](#)].
- [6] N.G. Deshpande and E. Ma, *Pattern of symmetry breaking with two Higgs doublets*, *Phys. Rev. D* **18** (1978) 2574 [[INSPIRE](#)].
- [7] R. Barbieri, L.J. Hall and V.S. Rychkov, *Improved naturalness with a heavy Higgs: an alternative road to LHC physics*, *Phys. Rev. D* **74** (2006) 015007 [[hep-ph/0603188](#)] [[INSPIRE](#)].
- [8] V. Silveira and A. Zee, *Scalar phantoms*, *Phys. Lett. B* **161** (1985) 136 [[INSPIRE](#)].
- [9] J. McDonald, *Gauge singlet scalars as cold dark matter*, *Phys. Rev. D* **50** (1994) 3637 [[hep-ph/0702143](#)] [[INSPIRE](#)].
- [10] C.P. Burgess, M. Pospelov and T. ter Veldhuis, *The minimal model of nonbaryonic dark matter: a singlet scalar*, *Nucl. Phys. B* **619** (2001) 709 [[hep-ph/0011335](#)] [[INSPIRE](#)].
- [11] XENON collaboration, *Dark matter search results from a one ton-year exposure of XENON1T*, *Phys. Rev. Lett.* **121** (2018) 111302 [[arXiv:1805.12562](#)] [[INSPIRE](#)].
- [12] PANDAX-4T collaboration, *Dark matter search results from the PandaX-4T commissioning run*, *Phys. Rev. Lett.* **127** (2021) 261802 [[arXiv:2107.13438](#)] [[INSPIRE](#)].
- [13] LZ collaboration, *First dark matter search results from the LUX-ZEPLIN (LZ) experiment*, *Phys. Rev. Lett.* **131** (2023) 041002 [[arXiv:2207.03764](#)] [[INSPIRE](#)].
- [14] T. Hambye and M.H.G. Tytgat, *Confined hidden vector dark matter*, *Phys. Lett. B* **683** (2010) 39 [[arXiv:0907.1007](#)] [[INSPIRE](#)].
- [15] T. Hambye, *Hidden vector dark matter*, *JHEP* **01** (2009) 028 [[arXiv:0811.0172](#)] [[INSPIRE](#)].
- [16] F. D’Eramo, M. McCullough and J. Thaler, *Multiple gamma lines from semi-annihilation*, *JCAP* **04** (2013) 030 [[arXiv:1210.7817](#)] [[INSPIRE](#)].
- [17] F. D’Eramo and J. Thaler, *Semi-annihilation of dark matter*, *JHEP* **06** (2010) 109 [[arXiv:1003.5912](#)] [[INSPIRE](#)].
- [18] G. Belanger, K. Kannike, A. Pukhov and M. Raidal, *Impact of semi-annihilations on dark matter phenomenology — an example of Z_N symmetric scalar dark matter*, *JCAP* **04** (2012) 010 [[arXiv:1202.2962](#)] [[INSPIRE](#)].
- [19] G. Bélanger, K. Kannike, A. Pukhov and M. Raidal, *Minimal semi-annihilating Z_N scalar dark matter*, *JCAP* **06** (2014) 021 [[arXiv:1403.4960](#)] [[INSPIRE](#)].
- [20] M. Kadastik, K. Kannike, A. Racioppi and M. Raidal, *Implications of dark matter direct detection results on LHC physics*, *Phys. Lett. B* **694** (2010) 242 [[arXiv:0912.3797](#)] [[INSPIRE](#)].

- [21] M. Kadastik, K. Kannike and M. Raidal, *Matter parity as the origin of scalar dark matter*, *Phys. Rev. D* **81** (2010) 015002 [[arXiv:0903.2475](#)] [[INSPIRE](#)].
- [22] M. Kadastik, K. Kannike and M. Raidal, *Dark matter as the signal of grand unification*, *Phys. Rev. D* **80** (2009) 085020 [*Erratum ibid.* **81** (2010) 029903] [[arXiv:0907.1894](#)] [[INSPIRE](#)].
- [23] M. Kadastik, K. Kannike, A. Racioppi and M. Raidal, *EWSB from the soft portal into dark matter and prediction for direct detection*, *Phys. Rev. Lett.* **104** (2010) 201301 [[arXiv:0912.2729](#)] [[INSPIRE](#)].
- [24] M. Aoki and T. Toma, *Impact of semi-annihilation of Z_3 symmetric dark matter with radiative neutrino masses*, *JCAP* **09** (2014) 016 [[arXiv:1405.5870](#)] [[INSPIRE](#)].
- [25] M. Kakizaki, A. Santa and O. Seto, *Phenomenological signatures of mixed complex scalar WIMP dark matter*, *Int. J. Mod. Phys. A* **32** (2017) 1750038 [[arXiv:1609.06555](#)] [[INSPIRE](#)].
- [26] G. Belanger, A. Mjallal and A. Pukhov, *Two dark matter candidates: the case of inert doublet and singlet scalars*, *Phys. Rev. D* **105** (2022) 035018 [[arXiv:2108.08061](#)] [[INSPIRE](#)].
- [27] G. Belanger, A. Mjallal and A. Pukhov, *WIMP and FIMP dark matter in the inert doublet plus singlet model*, *Phys. Rev. D* **106** (2022) 095019 [[arXiv:2205.04101](#)] [[INSPIRE](#)].
- [28] C.E. Yaguna and Ó. Zapata, *Multi-component scalar dark matter from a Z_N symmetry: a systematic analysis*, *JHEP* **03** (2020) 109 [[arXiv:1911.05515](#)] [[INSPIRE](#)].
- [29] A. Bas i Benito, J. Herrero-García and D. Vatsyayan, *Multi-component dark sectors: symmetries, asymmetries and conversions*, *JHEP* **10** (2022) 075 [[arXiv:2207.02874](#)] [[INSPIRE](#)].
- [30] C.E. Yaguna and Ó. Zapata, *Two-component scalar dark matter in Z_{2n} scenarios*, *JHEP* **10** (2021) 185 [[arXiv:2106.11889](#)] [[INSPIRE](#)].
- [31] D. Jurčiukonis and L. Lavoura, *The centers of discrete groups as stabilizers of dark matter*, *PTEP* **2023** (2023) 023B02 [[arXiv:2210.12133](#)] [[INSPIRE](#)].
- [32] G. Bélanger, A. Pukhov, C.E. Yaguna and Ó. Zapata, *The Z_7 model of three-component scalar dark matter*, *JHEP* **03** (2023) 100 [[arXiv:2212.07488](#)] [[INSPIRE](#)].
- [33] G. Belanger, K. Kannike, A. Pukhov and M. Raidal, *Z_3 scalar singlet dark matter*, *JCAP* **01** (2013) 022 [[arXiv:1211.1014](#)] [[INSPIRE](#)].
- [34] S. Bhattacharya, P. Ghosh, T.N. Maity and T.S. Ray, *Mitigating direct detection bounds in non-minimal Higgs portal scalar dark matter models*, *JHEP* **10** (2017) 088 [[arXiv:1706.04699](#)] [[INSPIRE](#)].
- [35] P. Ko and Y. Tang, *Self-interacting scalar dark matter with local Z_3 symmetry*, *JCAP* **05** (2014) 047 [[arXiv:1402.6449](#)] [[INSPIRE](#)].
- [36] P. Ko and Y. Tang, *Galactic center γ -ray excess in hidden sector DM models with dark gauge symmetries: local Z_3 symmetry as an example*, *JCAP* **01** (2015) 023 [[arXiv:1407.5492](#)] [[INSPIRE](#)].
- [37] S.-M. Choi and H.M. Lee, *SIMP dark matter with gauged Z_3 symmetry*, *JHEP* **09** (2015) 063 [[arXiv:1505.00960](#)] [[INSPIRE](#)].
- [38] E. Ma, N. Pollard, R. Srivastava and M. Zakeri, *Gauge $B - L$ model with residual Z_3 symmetry*, *Phys. Lett. B* **750** (2015) 135 [[arXiv:1507.03943](#)] [[INSPIRE](#)].
- [39] K. Kannike, K. Loos and M. Raidal, *Gravitational wave signals of pseudo-Goldstone dark matter in the Z_3 complex singlet model*, *Phys. Rev. D* **101** (2020) 035001 [[arXiv:1907.13136](#)] [[INSPIRE](#)].

- [40] W. Cheng, X. Liu and R. Zhou, *Non-minimal coupling inflation and dark matter under the Z_3 symmetry*, *JCAP* **05** (2023) 049 [[arXiv:2206.12624](#)] [[INSPIRE](#)].
- [41] A. Hektor, A. Hryczuk and K. Kannike, *Improved bounds on Z_3 singlet dark matter*, *JHEP* **03** (2019) 204 [[arXiv:1901.08074](#)] [[INSPIRE](#)].
- [42] Y. Cai and A.P. Spray, *The galactic center excess from Z_3 scalar semi-annihilations*, *JHEP* **06** (2016) 156 [[arXiv:1511.09247](#)] [[INSPIRE](#)].
- [43] G. Arcadi, F.S. Queiroz and C. Siqueira, *The semi-Hooperon: gamma-ray and anti-proton excesses in the galactic center*, *Phys. Lett. B* **775** (2017) 196 [[arXiv:1706.02336](#)] [[INSPIRE](#)].
- [44] F.S. Queiroz and C. Siqueira, *Search for semi-annihilating dark matter with Fermi-LAT, H.E.S.S., Planck, and the Cherenkov Telescope Array*, *JCAP* **04** (2019) 048 [[arXiv:1901.10494](#)] [[INSPIRE](#)].
- [45] Z. Kang, P. Ko and T. Matsui, *Strong first order EWPT & strong gravitational waves in Z_3 -symmetric singlet scalar extension*, *JHEP* **02** (2018) 115 [[arXiv:1706.09721](#)] [[INSPIRE](#)].
- [46] P. Athron et al., *Impact of vacuum stability, perturbativity and XENON1T on global fits of Z_2 and Z_3 scalar singlet dark matter*, *Eur. Phys. J. C* **78** (2018) 830 [[arXiv:1806.11281](#)] [[INSPIRE](#)].
- [47] B. Swiezewska and M. Krawczyk, *Diphoton rate in the inert doublet model with a 125 GeV Higgs boson*, *Phys. Rev. D* **88** (2013) 035019 [[arXiv:1212.4100](#)] [[INSPIRE](#)].
- [48] M. Krawczyk, D. Sokolowska, P. Swaczyna and B. Swiezewska, *Constraining inert dark matter by $R_{\gamma\gamma}$ and WMAP data*, *JHEP* **09** (2013) 055 [[arXiv:1305.6266](#)] [[INSPIRE](#)].
- [49] A. Belyaev et al., *Anatomy of the inert two Higgs doublet model in the light of the LHC and non-LHC dark matter searches*, *Phys. Rev. D* **97** (2018) 035011 [[arXiv:1612.00511](#)] [[INSPIRE](#)].
- [50] A. Belyaev et al., *Advancing LHC probes of dark matter from the inert two-Higgs-doublet model with the monojet signal*, *Phys. Rev. D* **99** (2019) 015011 [[arXiv:1809.00933](#)] [[INSPIRE](#)].
- [51] A. Goudelis, B. Herrmann and O. Stål, *Dark matter in the inert doublet model after the discovery of a Higgs-like boson at the LHC*, *JHEP* **09** (2013) 106 [[arXiv:1303.3010](#)] [[INSPIRE](#)].
- [52] M.A. Díaz, B. Koch and S. Urrutia-Quiroga, *Constraints to dark matter from inert Higgs doublet model*, *Adv. High Energy Phys.* **2016** (2016) 8278375 [[arXiv:1511.04429](#)] [[INSPIRE](#)].
- [53] N. Blinov, J. Kozaczuk, D.E. Morrissey and A. de la Puente, *Compressing the inert doublet model*, *Phys. Rev. D* **93** (2016) 035020 [[arXiv:1510.08069](#)] [[INSPIRE](#)].
- [54] I.F. Ginzburg, K.A. Kanishev, M. Krawczyk and D. Sokolowska, *Evolution of universe to the present inert phase*, *Phys. Rev. D* **82** (2010) 123533 [[arXiv:1009.4593](#)] [[INSPIRE](#)].
- [55] G. Gil, P. Chankowski and M. Krawczyk, *Inert dark matter and strong electroweak phase transition*, *Phys. Lett. B* **717** (2012) 396 [[arXiv:1207.0084](#)] [[INSPIRE](#)].
- [56] D. Borah and J.M. Cline, *Inert doublet dark matter with strong electroweak phase transition*, *Phys. Rev. D* **86** (2012) 055001 [[arXiv:1204.4722](#)] [[INSPIRE](#)].
- [57] J.M. Cline and K. Kainulainen, *Improved electroweak phase transition with subdominant inert doublet dark matter*, *Phys. Rev. D* **87** (2013) 071701 [[arXiv:1302.2614](#)] [[INSPIRE](#)].
- [58] N. Blinov, S. Profumo and T. Stefaniak, *The electroweak phase transition in the inert doublet model*, *JCAP* **07** (2015) 028 [[arXiv:1504.05949](#)] [[INSPIRE](#)].
- [59] S. Fabian, F. Goertz and Y. Jiang, *Dark matter and nature of electroweak phase transition with an inert doublet*, *JCAP* **09** (2021) 011 [[arXiv:2012.12847](#)] [[INSPIRE](#)].

- [60] N. Benincasa, L. Delle Rose, K. Kannike and L. Marzola, *Multi-step phase transitions and gravitational waves in the inert doublet model*, *JCAP* **12** (2022) 025 [[arXiv:2205.06669](#)] [[INSPIRE](#)].
- [61] M.D. Astros, S. Fabian and F. Goertz, *Minimal inert doublet benchmark for dark matter and the baryon asymmetry*, [arXiv:2307.01270](#) [[INSPIRE](#)].
- [62] P. Ghosh, T. Ghosh and S. Roy, *Interplay among gravitational waves, dark matter and collider signals in the singlet scalar extended type-II seesaw model*, *JHEP* **10** (2023) 057 [[arXiv:2211.15640](#)] [[INSPIRE](#)].
- [63] P. Gondolo and G. Gelmini, *Cosmic abundances of stable particles: improved analysis*, *Nucl. Phys. B* **360** (1991) 145 [[INSPIRE](#)].
- [64] T. Binder, T. Bringmann, M. Gustafsson and A. Hryczuk, *Early kinetic decoupling of dark matter: when the standard way of calculating the thermal relic density fails*, *Phys. Rev. D* **96** (2017) 115010 [Erratum *ibid.* **101** (2020) 099901] [[arXiv:1706.07433](#)] [[INSPIRE](#)].
- [65] M. Duch and B. Grzadkowski, *Resonance enhancement of dark matter interactions: the case for early kinetic decoupling and velocity dependent resonance width*, *JHEP* **09** (2017) 159 [[arXiv:1705.10777](#)] [[INSPIRE](#)].
- [66] T. Binder, T. Bringmann, M. Gustafsson and A. Hryczuk, *Dark matter relic abundance beyond kinetic equilibrium*, *Eur. Phys. J. C* **81** (2021) 577 [[arXiv:2103.01944](#)] [[INSPIRE](#)].
- [67] LIGO SCIENTIFIC and VIRGO collaborations, *GW151226: observation of gravitational waves from a 22-solar-mass binary black hole coalescence*, *Phys. Rev. Lett.* **116** (2016) 241103 [[arXiv:1606.04855](#)] [[INSPIRE](#)].
- [68] LIGO SCIENTIFIC and VIRGO collaborations, *Observation of gravitational waves from a binary black hole merger*, *Phys. Rev. Lett.* **116** (2016) 061102 [[arXiv:1602.03837](#)] [[INSPIRE](#)].
- [69] K. Kajantie, M. Laine, K. Rummukainen and M.E. Shaposhnikov, *Is there a hot electroweak phase transition at $m_H \gtrsim m_W$?*, *Phys. Rev. Lett.* **77** (1996) 2887 [[hep-ph/9605288](#)] [[INSPIRE](#)].
- [70] Y. Aoki, F. Csikor, Z. Fodor and A. Ukawa, *The endpoint of the first order phase transition of the SU(2) gauge Higgs model on a four-dimensional isotropic lattice*, *Phys. Rev. D* **60** (1999) 013001 [[hep-lat/9901021](#)] [[INSPIRE](#)].
- [71] E. Witten, *Cosmic separation of phases*, *Phys. Rev. D* **30** (1984) 272 [[INSPIRE](#)].
- [72] P.J. Steinhardt, *Relativistic detonation waves and bubble growth in false vacuum decay*, *Phys. Rev. D* **25** (1982) 2074 [[INSPIRE](#)].
- [73] C.J. Hogan, *Nucleation of cosmological phase transitions*, *Phys. Lett. B* **133** (1983) 172 [[INSPIRE](#)].
- [74] LISA collaboration, *Laser Interferometer Space Antenna*, [arXiv:1702.00786](#) [[INSPIRE](#)].
- [75] eLISA collaboration, *The gravitational universe*, [arXiv:1305.5720](#) [[INSPIRE](#)].
- [76] J. Crowder and N.J. Cornish, *Beyond LISA: exploring future gravitational wave missions*, *Phys. Rev. D* **72** (2005) 083005 [[gr-qc/0506015](#)] [[INSPIRE](#)].
- [77] V. Corbin and N.J. Cornish, *Detecting the cosmic gravitational wave background with the big bang observer*, *Class. Quant. Grav.* **23** (2006) 2435 [[gr-qc/0512039](#)] [[INSPIRE](#)].
- [78] W.-H. Ruan, Z.-K. Guo, R.-G. Cai and Y.-Z. Zhang, *Taiji program: gravitational-wave sources*, *Int. J. Mod. Phys. A* **35** (2020) 2050075 [[arXiv:1807.09495](#)] [[INSPIRE](#)].

- [79] W.-R. Hu and Y.-L. Wu, *The Taiji program in space for gravitational wave physics and the nature of gravity*, *Natl. Sci. Rev.* **4** (2017) 685 [INSPIRE].
- [80] TIANQIN collaboration, *TianQin: a space-borne gravitational wave detector*, *Class. Quant. Grav.* **33** (2016) 035010 [arXiv:1512.02076] [INSPIRE].
- [81] N. Seto, S. Kawamura and T. Nakamura, *Possibility of direct measurement of the acceleration of the universe using 0.1 Hz band laser interferometer gravitational wave antenna in space*, *Phys. Rev. Lett.* **87** (2001) 221103 [astro-ph/0108011] [INSPIRE].
- [82] S. Kawamura et al., *Current status of space gravitational wave antenna DECIGO and B-DECIGO*, *PTEP* **2021** (2021) 05A105 [arXiv:2006.13545] [INSPIRE].
- [83] P. Athron et al., *Cosmological phase transitions: from perturbative particle physics to gravitational waves*, *Prog. Part. Nucl. Phys.* **135** (2024) 104094 [arXiv:2305.02357] [INSPIRE].
- [84] S.R. Coleman and E.J. Weinberg, *Radiative corrections as the origin of spontaneous symmetry breaking*, *Phys. Rev. D* **7** (1973) 1888 [INSPIRE].
- [85] C. Delaunay, C. Grojean and J.D. Wells, *Dynamics of non-renormalizable electroweak symmetry breaking*, *JHEP* **04** (2008) 029 [arXiv:0711.2511] [INSPIRE].
- [86] J.M. Cline, K. Kainulainen and M. Trott, *Electroweak baryogenesis in two Higgs doublet models and B meson anomalies*, *JHEP* **11** (2011) 089 [arXiv:1107.3559] [INSPIRE].
- [87] L. Dolan and R. Jackiw, *Symmetry behavior at finite temperature*, *Phys. Rev. D* **9** (1974) 3320 [INSPIRE].
- [88] D.J. Gross, R.D. Pisarski and L.G. Yaffe, *QCD and instantons at finite temperature*, *Rev. Mod. Phys.* **53** (1981) 43 [INSPIRE].
- [89] R.R. Parwani, *Resummation in a hot scalar field theory*, *Phys. Rev. D* **45** (1992) 4695 [Erratum *ibid.* **48** (1993) 5965] [hep-ph/9204216] [INSPIRE].
- [90] M.E. Carrington, *The effective potential at finite temperature in the Standard Model*, *Phys. Rev. D* **45** (1992) 2933 [INSPIRE].
- [91] J.M. Cline and P.-A. Lemieux, *Electroweak phase transition in two Higgs doublet models*, *Phys. Rev. D* **55** (1997) 3873 [hep-ph/9609240] [INSPIRE].
- [92] E. Braaten and R.D. Pisarski, *Simple effective Lagrangian for hard thermal loops*, *Phys. Rev. D* **45** (1992) R1827 [INSPIRE].
- [93] K. Enqvist, A. Riotto and I. Vilja, *Baryogenesis and the thermalization rate of stop*, *Phys. Lett. B* **438** (1998) 273 [hep-ph/9710373] [INSPIRE].
- [94] J.R. Espinosa, M. Quiros and F. Zwirner, *On the nature of the electroweak phase transition*, *Phys. Lett. B* **314** (1993) 206 [hep-ph/9212248] [INSPIRE].
- [95] C. Manuel, *On the thermal gauge boson masses of the electroweak theory in the broken phase*, *Phys. Rev. D* **58** (1998) 016001 [hep-ph/9801364] [INSPIRE].
- [96] J. Bernon, L. Bian and Y. Jiang, *A new insight into the phase transition in the early universe with two Higgs doublets*, *JHEP* **05** (2018) 151 [arXiv:1712.08430] [INSPIRE].
- [97] R.N. Lerner and J. McDonald, *Gauge singlet scalar as inflaton and thermal relic dark matter*, *Phys. Rev. D* **80** (2009) 123507 [arXiv:0909.0520] [INSPIRE].
- [98] S. Kanemura, T. Kubota and E. Takasugi, *Lee-Quigg-Thacker bounds for Higgs boson masses in a two doublet model*, *Phys. Lett. B* **313** (1993) 155 [hep-ph/9303263] [INSPIRE].

- [99] A.G. Akeroyd, A. Arhrib and E.-M. Naimi, *Note on tree level unitarity in the general two Higgs doublet model*, *Phys. Lett. B* **490** (2000) 119 [[hep-ph/0006035](#)] [[INSPIRE](#)].
- [100] K. Kannike, *Vacuum stability of a general scalar potential of a few fields*, *Eur. Phys. J. C* **76** (2016) 324 [*Erratum ibid.* **78** (2018) 355] [[arXiv:1603.02680](#)] [[INSPIRE](#)].
- [101] Q.-H. Cao, E. Ma and G. Rajasekaran, *Observing the dark scalar doublet and its impact on the Standard-Model Higgs boson at colliders*, *Phys. Rev. D* **76** (2007) 095011 [[arXiv:0708.2939](#)] [[INSPIRE](#)].
- [102] E. Lundstrom, M. Gustafsson and J. Edsjo, *The inert doublet model and LEP II limits*, *Phys. Rev. D* **79** (2009) 035013 [[arXiv:0810.3924](#)] [[INSPIRE](#)].
- [103] A. Pierce and J. Thaler, *Natural dark matter from an unnatural Higgs boson and new colored particles at the TeV scale*, *JHEP* **08** (2007) 026 [[hep-ph/0703056](#)] [[INSPIRE](#)].
- [104] CMS collaboration, *A search for decays of the Higgs boson to invisible particles in events with a top-antitop quark pair or a vector boson in proton-proton collisions at $\sqrt{s} = 13$ TeV*, *Eur. Phys. J. C* **83** (2023) 933 [[arXiv:2303.01214](#)] [[INSPIRE](#)].
- [105] ATLAS collaboration, *Combination of searches for invisible decays of the Higgs boson using 139 fb^{-1} of proton-proton collision data at $\sqrt{s} = 13$ TeV collected with the ATLAS experiment*, *Phys. Lett. B* **842** (2023) 137963 [[arXiv:2301.10731](#)] [[INSPIRE](#)].
- [106] CMS collaboration, *Measurements of Higgs boson production cross sections and couplings in the diphoton decay channel at $\sqrt{s} = 13$ TeV*, *JHEP* **07** (2021) 027 [[arXiv:2103.06956](#)] [[INSPIRE](#)].
- [107] J. Haller et al., *Update of the global electroweak fit and constraints on two-Higgs-doublet models*, *Eur. Phys. J. C* **78** (2018) 675 [[arXiv:1803.01853](#)] [[INSPIRE](#)].
- [108] W. Grimus, L. Lavoura, O.M. Ogreid and P. Osland, *The oblique parameters in multi-Higgs-doublet models*, *Nucl. Phys. B* **801** (2008) 81 [[arXiv:0802.4353](#)] [[INSPIRE](#)].
- [109] W. Grimus, L. Lavoura, O.M. Ogreid and P. Osland, *A precision constraint on multi-Higgs-doublet models*, *J. Phys. G* **35** (2008) 075001 [[arXiv:0711.4022](#)] [[INSPIRE](#)].
- [110] G. Bélanger, A. Pukhov, C.E. Yaguna and Ó. Zapata, *The Z_5 model of two-component dark matter*, *JHEP* **09** (2020) 030 [[arXiv:2006.14922](#)] [[INSPIRE](#)].
- [111] G. Bélanger et al., *micrOMEGAs5.0: freeze-in*, *Comput. Phys. Commun.* **231** (2018) 173 [[arXiv:1801.03509](#)] [[INSPIRE](#)].
- [112] G. Belanger, A. Mjallal and A. Pukhov, *Recasting direct detection limits within micrOMEGAs and implication for non-standard dark matter scenarios*, *Eur. Phys. J. C* **81** (2021) 239 [[arXiv:2003.08621](#)] [[INSPIRE](#)].
- [113] G. Alguero, G. Belanger, S. Kraml and A. Pukhov, *Co-scattering in micrOMEGAs: a case study for the singlet-triplet dark matter model*, *SciPost Phys.* **13** (2022) 124 [[arXiv:2207.10536](#)] [[INSPIRE](#)].
- [114] G. Belanger, F. Boudjema, A. Pukhov and A. Semenov, *micrOMEGAs3: a program for calculating dark matter observables*, *Comput. Phys. Commun.* **185** (2014) 960 [[arXiv:1305.0237](#)] [[INSPIRE](#)].
- [115] A. Hryczuk and M. Laletin, *Impact of dark matter self-scattering on its relic abundance*, *Phys. Rev. D* **106** (2022) 023007 [[arXiv:2204.07078](#)] [[INSPIRE](#)].
- [116] T. Bringmann and S. Hofmann, *Thermal decoupling of WIMPs from first principles*, *JCAP* **04** (2007) 016 [*Erratum ibid.* **03** (2016) E02] [[hep-ph/0612238](#)] [[INSPIRE](#)].

- [117] T. Binder et al., *Matter power spectrum in hidden neutrino interacting dark matter models: a closer look at the collision term*, *JCAP* **11** (2016) 043 [[arXiv:1602.07624](#)] [[INSPIRE](#)].
- [118] *Implementation of Boltzmann equation GitHub repository*, <http://github.com/dkaramit/BoltzmannEquation>.
- [119] J. Edsjo and P. Gondolo, *Neutralino relic density including coannihilations*, *Phys. Rev. D* **56** (1997) 1879 [[hep-ph/9704361](#)] [[INSPIRE](#)].
- [120] V. Shtabovenko, R. Mertig and F. Orellana, *FeynCalc 9.3: new features and improvements*, *Comput. Phys. Commun.* **256** (2020) 107478 [[arXiv:2001.04407](#)] [[INSPIRE](#)].
- [121] R.N. Mohapatra and G. Senjanovic, *Soft CP violation at high temperature*, *Phys. Rev. Lett.* **42** (1979) 1651 [[INSPIRE](#)].
- [122] R.N. Mohapatra and G. Senjanovic, *Broken symmetries at high temperature*, *Phys. Rev. D* **20** (1979) 3390 [[INSPIRE](#)].
- [123] S. Weinberg, *Gauge and global symmetries at high temperature*, *Phys. Rev. D* **9** (1974) 3357 [[INSPIRE](#)].
- [124] C. Caprini et al., *Science with the space-based interferometer eLISA. II: gravitational waves from cosmological phase transitions*, *JCAP* **04** (2016) 001 [[arXiv:1512.06239](#)] [[INSPIRE](#)].
- [125] H.-K. Guo, K. Sinha, D. Vagie and G. White, *The benefits of diligence: how precise are predicted gravitational wave spectra in models with phase transitions?*, *JHEP* **06** (2021) 164 [[arXiv:2103.06933](#)] [[INSPIRE](#)].
- [126] J.R. Espinosa, T. Konstandin, J.M. No and G. Servant, *Energy budget of cosmological first-order phase transitions*, *JCAP* **06** (2010) 028 [[arXiv:1004.4187](#)] [[INSPIRE](#)].
- [127] L. Niemi, M.J. Ramsey-Musolf, T.V.I. Tenkanen and D.J. Weir, *Thermodynamics of a two-step electroweak phase transition*, *Phys. Rev. Lett.* **126** (2021) 171802 [[arXiv:2005.11332](#)] [[INSPIRE](#)].
- [128] T. Biekötter et al., *The trap in the early universe: impact on the interplay between gravitational waves and LHC physics in the 2HDM*, *JCAP* **03** (2023) 031 [[arXiv:2208.14466](#)] [[INSPIRE](#)].
- [129] C. Grojean and G. Servant, *Gravitational waves from phase transitions at the electroweak scale and beyond*, *Phys. Rev. D* **75** (2007) 043507 [[hep-ph/0607107](#)] [[INSPIRE](#)].
- [130] M. Kamionkowski, A. Kosowsky and M.S. Turner, *Gravitational radiation from first order phase transitions*, *Phys. Rev. D* **49** (1994) 2837 [[astro-ph/9310044](#)] [[INSPIRE](#)].
- [131] C.J. Hogan, *Gravitational radiation from cosmological phase transitions*, *Mon. Not. Roy. Astron. Soc.* **218** (1986) 629.
- [132] M. Hindmarsh, S.J. Huber, K. Rummukainen and D.J. Weir, *Gravitational waves from the sound of a first order phase transition*, *Phys. Rev. Lett.* **112** (2014) 041301 [[arXiv:1304.2433](#)] [[INSPIRE](#)].
- [133] C. Caprini, R. Durrer and G. Servant, *The stochastic gravitational wave background from turbulence and magnetic fields generated by a first-order phase transition*, *JCAP* **12** (2009) 024 [[arXiv:0909.0622](#)] [[INSPIRE](#)].
- [134] M. Lewicki and V. Vaskonen, *Gravitational waves from bubble collisions and fluid motion in strongly supercooled phase transitions*, *Eur. Phys. J. C* **83** (2023) 109 [[arXiv:2208.11697](#)] [[INSPIRE](#)].
- [135] D. Croon et al., *Theoretical uncertainties for cosmological first-order phase transitions*, *JHEP* **04** (2021) 055 [[arXiv:2009.10080](#)] [[INSPIRE](#)].

- [136] P. Athron et al., *How arbitrary are perturbative calculations of the electroweak phase transition?*, *JHEP* **01** (2023) 050 [[arXiv:2208.01319](#)] [[INSPIRE](#)].
- [137] S.J. Huber and T. Konstandin, *Gravitational wave production by collisions: more bubbles*, *JCAP* **09** (2008) 022 [[arXiv:0806.1828](#)] [[INSPIRE](#)].
- [138] M. Lewicki and V. Vaskonen, *On bubble collisions in strongly supercooled phase transitions*, *Phys. Dark Univ.* **30** (2020) 100672 [[arXiv:1912.00997](#)] [[INSPIRE](#)].
- [139] M. Lewicki and V. Vaskonen, *Gravitational wave spectra from strongly supercooled phase transitions*, *Eur. Phys. J. C* **80** (2020) 1003 [[arXiv:2007.04967](#)] [[INSPIRE](#)].
- [140] M. Lewicki and V. Vaskonen, *Gravitational waves from colliding vacuum bubbles in gauge theories*, *Eur. Phys. J. C* **81** (2021) 437 [*Erratum ibid.* **81** (2021) 1077] [[arXiv:2012.07826](#)] [[INSPIRE](#)].
- [141] M. Hindmarsh, S.J. Huber, K. Rummukainen and D.J. Weir, *Shape of the acoustic gravitational wave power spectrum from a first order phase transition*, *Phys. Rev. D* **96** (2017) 103520 [*Erratum ibid.* **101** (2020) 089902] [[arXiv:1704.05871](#)] [[INSPIRE](#)].
- [142] C. Caprini et al., *Detecting gravitational waves from cosmological phase transitions with LISA: an update*, *JCAP* **03** (2020) 024 [[arXiv:1910.13125](#)] [[INSPIRE](#)].
- [143] K. Schmitz, *LISA sensitivity to gravitational waves from sound waves*, *Symmetry* **12** (2020) 1477 [[arXiv:2005.10789](#)] [[INSPIRE](#)].
- [144] H.-K. Guo, K. Sinha, D. Vagie and G. White, *Phase transitions in an expanding universe: stochastic gravitational waves in standard and non-standard histories*, *JCAP* **01** (2021) 001 [[arXiv:2007.08537](#)] [[INSPIRE](#)].
- [145] J. Ellis, M. Lewicki, J.M. No and V. Vaskonen, *Gravitational wave energy budget in strongly supercooled phase transitions*, *JCAP* **06** (2019) 024 [[arXiv:1903.09642](#)] [[INSPIRE](#)].
- [146] K. Schmitz, *New sensitivity curves for gravitational-wave signals from cosmological phase transitions*, *JHEP* **01** (2021) 097 [[arXiv:2002.04615](#)] [[INSPIRE](#)].
- [147] XENON collaboration, *Projected WIMP sensitivity of the XENONnT dark matter experiment*, *JCAP* **11** (2020) 031 [[arXiv:2007.08796](#)] [[INSPIRE](#)].
- [148] E. Thrane and J.D. Romano, *Sensitivity curves for searches for gravitational-wave backgrounds*, *Phys. Rev. D* **88** (2013) 124032 [[arXiv:1310.5300](#)] [[INSPIRE](#)].
- [149] A. Azatov, D. Barducci and F. Sgarlata, *Gravitational traces of broken gauge symmetries*, *JCAP* **07** (2020) 027 [[arXiv:1910.01124](#)] [[INSPIRE](#)].
- [150] M. Mulders and C. Duhr, *Proceedings, 2018 European School of High-Energy Physics (ESHEP 2018): Maratea, Italy, June 20–July 3 2018*, CERN, Geneva, Switzerland (2019) [[DOI:10.23730/CYRSP-2019-006](#)] [[INSPIRE](#)].
- [151] G.B. Gelmini, *Cosmology and astroparticles*, *AIP Conf. Proc.* **359** (1996) 148 [[hep-ph/9606409](#)] [[INSPIRE](#)].
- [152] K. Akita and M. Yamaguchi, *A review of neutrino decoupling from the early universe to the current universe*, *Universe* **8** (2022) 552 [[arXiv:2210.10307](#)] [[INSPIRE](#)].